- Spectropolarimetry -

A new Window for Stellar Physics

Thomas Eversberg

Département de Physique,
Université de Montréal
C.P. 6128, Succ. Centre Ville
Montréal H3C 3J7

November 7, 1999

Contents

Chapter 1

Introduction

Ever since man has observed the sky he has tried to get more and more knowledge about the nature of the contents in the Universe. But we have a fundamental problem: the size of this laboratory. Most bodies that we wish to investigate are found at large distances. Neglecting the solar system, a real in-situ measurement in another stellar system will perhaps never be possible. To find out what kind of physical mechanisms lead to the phenomena we see, we have only one tool: the radiation of these objects in the form of electromagnetic and sometimes partical beams. In addition, the distances are often so extreme, that even the largest stars with diameters greater than that of Mars' orbit are no resolvable in our largest telescopes. Only recent observations with state-of-the-art technology made direct imaging of stars available.

A first attempt to understand the physics of the Universe was by measuring the intensity of light. This has been done for centuries. An extreme example is the visual observation of an exploding star, a supernova, by Chinese astronomers in the Taurus constellation in 1054. Measuring the light intensity visually in this way can be done with surprisingly high accuracy. For instance, the human eye can detect variations of as good as a tenth of a magnitude.

A later attempt involved measuring the spectral behavior of light. Since we know that white light is composed of colors and since Fraunhofer found absorption features in the solar spectrum, we can gain more information about stars far away by applying the techniques of spectroscopy to them. And after modern quantum mechanics was developed in the 1920's we have a powerful and very succesful tool to study global as well as localized structures in stellar surfaces or atmospheres.

In actual fact the second attempt is only an extension of the first one. A spectrum is just measuring the light intensity as it depends on the wavelength. Another possibility is using a fundamental property of light which has been known for some 300 years: Light can be *polarized*. Because light is nothing other than an electromagnetic wave, its electric field vectors can oscillate e.g. in one plane. Therefore, if we observe stars only with respect to their intensity spectra, we ignore a very large portion of the total information, and it is surprising that it has only been known since 1948 that a majority of stars is partially plane polarized.

Since then, many polarimetric surveys have been done for other objects in the Universe beside stars (e.g., planets, comets and galaxies). For some of those surveys circularly polarized light was also measured, with considerable success in detecting magnetic fields.

It is clear that the next step should be from wavelength independent polarization to wavelength dependent *spectropolarization*. This has been done very little until now and should open a broad window for obtaining information about stars, especially about early-type stars with their strongly extended atmospheres, capable of enhanced polarization.

An overview of the spectropolarimetric results of observing and modelling of these stars will be the content of this report.

Chapter 2

Polarized light in nature

2.1 Historical background

Polarized light is one of nature's ultimate phenomena. A monochromatic, *polarized* ray cannot be subdivided into simpler components: no simpler components exist. The process of analysis can advance no further as far as anyone knows.

There is much to be gained, however, by considering how a beam of polarized light behaves and how it may be depicted. When such a beam encounters a birefringent crystal, a dichroic film, or an oblique dielectric surface, a great variety of behavior depending on the physical origins or their detection may result.

The history of man's understanding of polarized light has been touched on by many authors, e.g., Preston (1928) [56] or Partington (1953) [51]. The following table lists some principal advances (after Shurcliff, 1962 [74]):

- 1669 - Erasmus Bartholinus discovered double refraction.
- 1690 - Christian Huygens discovered polarization of light.
- 1757 - Robert Hook suggested that light vibrations are transverse.
- 1808 - Etienne-Louise Malus discovered polarization by reflection.
- 1812 - David Brewster discovered "Brewster's law".
- 1816 - Augustin Fresnel found that two rays that are polarized at right angles cannot interfere.
- 1828 - William Nicol invented the Nicol prism.
- 1845 - Michael Faraday discovered the "Faraday effect".
- 1852 - George Stokes invented the four Stokes parameters.
- 1875 - John Kerr discoverd the "Kerr" effect.
- 1892 - Henri Poincaré invented the "Poincaré-sphere" method.
- 1933 - Bernard Lyot invented the polarization-type, narrow-band filter that now bears his name.
- 1943 - Hans Mueller invented a phenomenological approach to problems involving polarized light by use of 4×4 matrices.
- 1949 - Hall and Hiltner independently discovered stellar polarization.

2.2 Mechanisms producing polarized light

In nature we find a number of effects which can produce polarized light, some of high interest for applying in optical measurements (after Shurcliff, 1962 [74]):

- *Stark Effect.* If a plasma emits light in the region of a strong electric field **F**, this light is polarized in the direction perpendicular to the field direction. Each spectral line is split by the field into several lines, and these exhibit polarization. Light emitted perpendicular to **F** consists of lines that are linearly polarized with the electric vibration either parallel to **F** (the p-component) or perpendicular to it (the s-component); this is called the transverse Stark effect. Light emitted parallel to **F** is unpolarized.
- *Zeeman effect.* If a plasma emits light in the region of a strong magnetic field **B** a typical spectral line is split into several lines. Light emitted perpendicular to **B** is linear polarized with vibration direction parallel to **B** (p-component) or perpendicular to **B** (s-component); this is the transverse Zeeman effect. Light emitted parallel to **B** is circularly polarized; this is the longitudinal Zeeman effect.
- *Cerenkov effect.* When relativistic electrons travel through a medium and move (temporarily) faster than the light velocity in this medium, the material will emit light. The wavefront of this light is conical and each ray is linearly polarized with the direction of its electric vibration parallel to the pertinent element of the wavefront.
- *Scattering on small particles.* If a light beam scatters on small particles (Rayleigh scattering) this beam is polarized. The effect is seen as the polarization of the sky and the interstellar medium.
- *Cyclotron radiation.* If non-relativistic electrons are captured by a strong magnetic field **B** and spin around the field lines, they emit Bremsstrahlung which is linearly polarized perpendicular to **B**. The beam angle is directly correlated with the kinetic energy of the electrons.
- *Other methods.* There are several other effects which can produce polarized light. Briefly mentioned are the *Grating plus electron beam* (Smith

& Purcell (1953) [76], the *Undulator* (Motz et al., 1953 [49]), *Light from canal rays*, and *K-capture* of high-energy gamma-rays (Hartwig & Schopper, 1959 [26]).

2.3 Astronomical polarimetry

According to the above listed polarization effects one can expect several sources of polarization in the Universe. In this context we can distinguish between the polarization of extended sources (the Sun, planets, comets, the interstellar medium, nebulae and galaxies) and point sources (distant stars). A brief list of optical phenomena which are responsible for observed polarization in astronomical objects is given by Serkowski (1974) [70]:

- *reflection from solid surfaces*: moon, Mars, Mercury, minor planets
- *scattering by small grains*: zodiacal light, comets, Venus, Jupiter, reflection nebulae, atmospheres of late-type stars, spiral galaxies, interstellar polarization of starlight
- *scattering by molecules* (Rayleigh scattering): Jupiter and outer planets, Venus
- *scattering by free electrons* (Thomson scattering): solar corona, envelopes of early-type stars
- *Hanle effect* (resonance scattering of bound electrons in magnetic fields): solar chromosphere and corona
- *Zeeman effect*: sunspots and magnetic stars, interstellar medium
- *grey-body magnetoemission*: white dwarfs
- *gyro-resonance emission*: solar chromosphere and corona
- *synchrotron emission*: Jupiter, Crab nebula, pulsars, galactic background radio emission, radio galaxies, quasars

For hot stars, mainly those mechanisms play a role that can survive the tremendous radiation field with temperatures of up to several tens of thousands of degrees. These involve mainly Thomson scattering and the Zeeman effect. In late-type stars, dust plays a role, so that scattering on small grains is not neglegible in such stars.

This report will concentrate on the polarimetry of hot stars.

Chapter 3

The Stokes parameters

Most information we can gain about the stars is obtained by measuring their radiation. Because of the enormous distances, stellar light reaches us in the form of a parallel bundle of radiation and no two-dimensional information is obtainable at least in most cases, even if astronomers may be on the brink of a resolution break through. The complete description of a stellar beam is established by the following characteristics:

- the direction of the beam described by its coordinates, e.g., in the equatorial system, α and δ,
- the flux F of the incoming light, and
- the status of polarization, described by the Stokes parameters Q, U and V.

The flux and the polarization are, in general, a function of the wavelength.

3.1 Description of polarization with the Stokes parameters

In 1852 Sir George Stokes introduced the four Stokes parameters I, Q, U and V to describe polarized light in an easy way:

One can choose a coordinate system by considering an electromagnetic wave of a single photon ray * where the two mutual perpendiculer vectors l and r lies in a fixed plane and $l \times r$ is in the propagation direction of this wave (Fig. 3.1). If furthermore l lies in the plane of the meridian of an equatorial coordinate system, we can describe the components of the electric vector E as a function of time with:

$$E_l = E_{l0} \sin(\omega t - \epsilon_l) \quad (3.1)$$

$$E_r = E_{r0} \sin(\omega t - \epsilon_r) \quad (3.2)$$

*To consider a single photon, we have to use expressions of quantum electro-dynamics: A single photon is only circularly polarized, which follows from its helicity. The polarization vector represents the "spin function" of a photon. Any polarization can be expressed by two orthogonal polarizations in the form of a linear combination of these two directions where the square of the amplitude of the coefficients gives the probabilities for the polarization directions. The complete discription of a polarized photon is given by its polarisation matrix (a hermitic tensor of 2nd stage) with Lorentz invariant components.

(ω = angular frequency, E_{l0}, E_{r0} = wave amplitudes, ϵ_l, ϵ_r = phases).

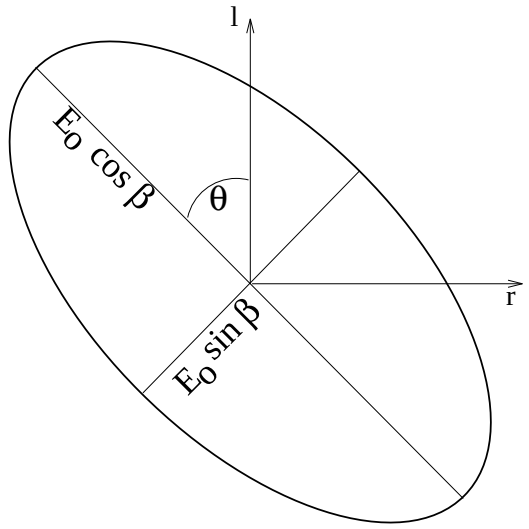

Figure 3.1: Parameters defining the polarization of a simple wave. The light is coming toward us and l lies in the plane of the meridian of the equatorial coordinate system and directed towards the northern hemisphere(Serkowski, 1962).

From these two equations one can see that the vector E describes an ellipse in the plane of l and r. If Θ is the angle between the long axis of the ellipse and the direction of l, and $\sin\beta$ and $\cos\beta$ are the short and the long half-axis of the ellipse, respectively, one can define the Stokes parameters in the following manner (e.g., Chandrasekhar, 1950 [13]):

$$I = E_{lo}^2 + E_{ro}^2 = \sqrt{Q^2 + U^2 + V^2} \quad (3.3)$$

$$Q = E_{lo}^2 - E_{ro}^2 = I \cos 2\beta \cos 2\Theta \quad (3.4)$$

$$U = -2E_{l0}E_{r0} \cos(\epsilon_l - \epsilon_r) = I \cos 2\beta \sin 2\Theta \quad (3.5)$$

$$V = 2E_{l0}E_{r0} \sin(\epsilon_l - \epsilon_r) = I \sin 2\beta. \quad (3.6)$$

Note that for another coordinate system, only Θ changes; I and β are *invariant* with respect to a change of the coordinate system and hence also $Q^2 + U^2$ and V are invariants.

3.2 Properties of Stoke parameters

Because of the *additivity* of the Stokes parameters (Stokes parameters discribing light are sums of the corresponding Stokes parameters discribing the "simple waves" of which the light is composed) light can always be decomposed into two beams:

1. Unpolarized light with $Q = U = V = 0$ and
2. fully elliptical polarized light of intensity $\sqrt{Q^2 + U^2 + V^2}$.

The degree of polarization is described by

$$P = \frac{\sqrt{Q^2 + U^2}}{I} = \cos 2\beta \tag{3.7}$$

and the degree of ellipticity by

$$P_v = \frac{|V|}{I} = \sin 2\beta. \tag{3.8}$$

It is possible to split partially polarized light ($V = 0$) into two beams of fully plane polarized light. The first E vector then makes an angle Θ to the direction l, described by I_{max}, and the second E vector makes an angle $\Theta + 90^\circ$, described by I_{min}.

In the case of electron (Thomson) scattering the scattering process changes the length of the electric vector as described in Fig. 3.2

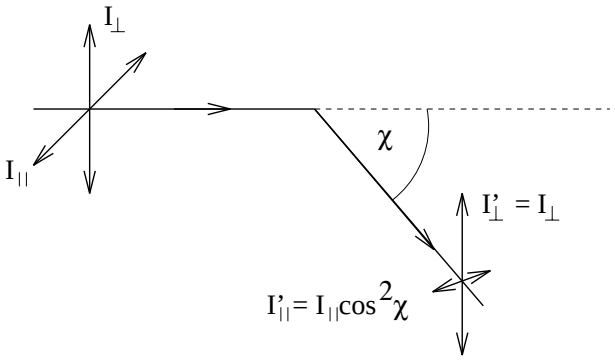

Figure 3.2: The electron scattering process. The intensity of the electric vector is reduced by $\cos^2 \chi$ for the component parallel to the scattering plane. The perpendicular component is unaltered after scattering. χ is the scattering angle.

The degree of polarization after scattering is

$$P = \frac{I_\perp - I_\parallel}{I_\perp + I_\parallel} = \frac{1 - \cos^2 \chi}{1 + \cos^2 \chi}. \tag{3.9}$$

The polarization position angle, Θ, is the position of the maximized electric vector, which gives the direction of the scattering plane. So one can describe the polarization as a "quasi vector" with magnitude P and direction χ. But these parameters (P,χ) do not follow normal vector addition and one has to use the Stokes parameters which add linearly. The Stokes parameters are sums and differences of the intensity of the radiation field measured along different axes and one can understand them in the following way:

- I is the total intensity of the radiation field.
- Q is the intensity difference between components of the electric vector along two orthogonal directions.
- U is the intensity difference between components of the electric vector along two orthogonal axes rotated through 45° from the Q direction.
- V is the intensity difference between the left and right circularly polarized components.

Chapter 4

Polarimetric diagnostics of hot stars

4.1 Interstellar polarization

After the description of possible intrinsic polarization in hot-star binaries by Chandrasekhar (1946 [11] und 1947 [12]), Hiltner (1949) [30] and Hall (1949) [22] discovered interstellar linear polarization. The interstellar gas component consists mainly of atoms, ions and molecules of hydrogen. Until the discover of interstellar polarization it was believed that the dust component was spherically symmetric. But it became clear that the degree of polarization is correlated with the extinction and the difference between the extinction coefficient for two mutually perpendicular oscillating light beams can be up to 6%. The highest degree of polarization lies in the galactic plane and we find regions where the polarization direction is strongly correlated. The variation of the degree of polarization between $0.33\,\mu$ (3300 Å) and $1\,\mu$ is relatively small. In general, $P(\lambda)$ reveals a fairly flat curve with its maximum between 5000 Å and 7000 Å. For this dependence, Serkowski (1975 [73]) found an empirical relation between $P(\lambda)/P_{max}$ and λ_{max}/λ which is shown as a plot in Fig. 4.1.

$$\frac{P(\lambda)}{P_{max}} = e^{-1.15\ln^2(\lambda_{max}/\lambda)}. \qquad (4.1)$$

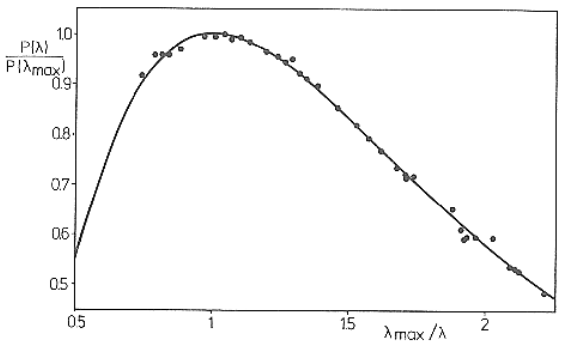

Figure 4.1: Wavelength dependence of interstellar linear polarization of stellar light according to Serkowsi (1975).

In addition, observations showed that the distribution of the interstellar polarization is not regular. However, a maximum is found in the galactic plane and polarization vectors are in parts strongly aligned and not stochastic. This can be understood by the idea that the polarization is introduced by light which is scattered off *non-spherical grains* which are aligned with the magnetic field of our galaxy with a strength of some 10^{-6} G.

This means that measurements of stellar polarization can never neglect the influence of the polarization of the material between the star and the observer. Such measurements must be corrected for interstellar polarization.

4.2 Intrinsic linear polarization; wavelength- and time dependence

Intrinsic polarization of early-type stars arises mainly from Thomson (electron) scattering (see 2.3) of stellar light. The fundamental condition to show any intrinsic polarization and/or polarimetric variability is a non spherical stellar atmosphere. If spherical geometry prevails, all polarization due to Thomson scattering cancels out. But if any deviation from a radial sphere exists (e.g., an equatorial disk or localized regions of higher ionic or atomic density, so called *blobs*, or only density enhancement above the equator) an observer should be able to detect intrinsic polarization.

Chandrasekhar (1946 [11]) predicted intrinsic polarization values for a stellar disk to be zero at the center and as high as $\sim$ 11% at the limb. The electric vector is then vibrating tangentially to the stellar surface. To estimate the asymmetric geometry of the star-envelope system via spectropolarimetry one has to consider the expected degree of polarization.

Polarization in early-type stars often yields intrinsic variability in time and sometimes with wavelengths.

(A) Wavelength dependence

Nordsieck et al. (1992 [52]) showed four different explanations how the observed polarization becomes wavelength dependent and also Schulte-Ladbeck et al.

(1992) [67] gave a brief explanation for this behavior and the physical reasons.

If the star and the scattered light are both in the observer's beam, and the polarized scattered light L_{scat} is small compared to the direct unpolarized starlight $L_\star$ (Fig. 4.2), the observed degree of polarization p_{obs} is

$$p_{obs} = p(\Theta)L_{scat}/(L_\star + L_{scat}) \quad (4.2)$$

$$\approx \frac{\Omega}{4\pi} p_{max} g(\Theta)\tau_s(1-\tau_s)D(r)\sin^2\Theta, \quad (4.3)$$

where Ω is the solid angle subtended at the star by the scatterer, p_{max} is the polarization near $\Theta = 90°$, $g(\Theta)$ is the scattering efficiency, τ_s is the scattering optical depth, and D(r) is the geometry dilution due to the finite star size.

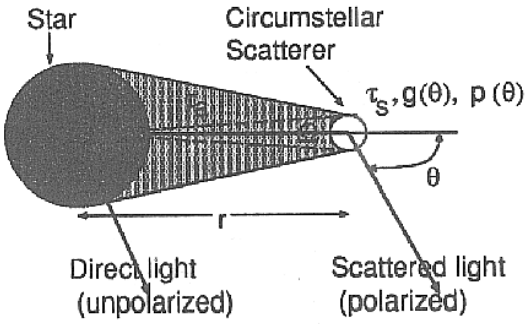

Figure 4.2: Intrinsic polarization from circumstellar envelopes (Nordsieck et al., 1992).

Figure 4.3 illustrates the four basic ways of making p_{obs} wavelength dependent.

(a) Unpolarized light L_{dil} not originating in the star (e.g., nebular emission from circumstellar material) dilutes the polarized light:

$$p_{obs} = p(\Theta)L_{scat}/(L_\star + L_{scat} + L_{dil}), \quad (4.4)$$

where $L_{dil}(\lambda)$ is wavelength dependent.

(b) Absorptive opacity may reduce scattered light more than direct starlight:

$$p_{obs} \sim 1 - \tau_a(\lambda) \quad (4.5)$$

and we observe polarization with features that are weak or do not exist in the stellar spectrum.

(c) Different illumination geometry in different wavelengths (e.g., due to limb darkening):

$$p_{obs} \sim D(\lambda)\sin^2\Theta(\lambda). \quad (4.6)$$

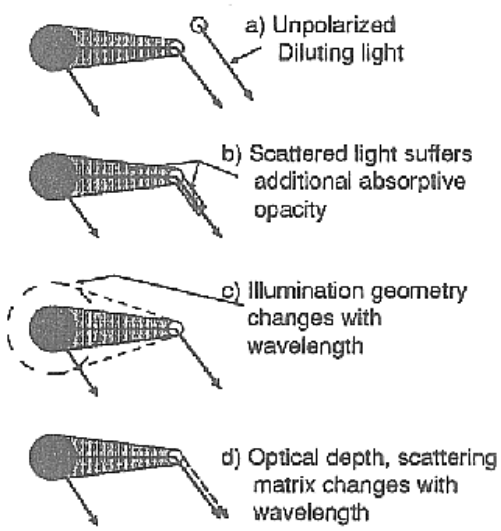

Figure 4.3: Sources of spectropolarimetric features (Nordsieck et al., 1992).

(d) The scattering process may itself be wavelength dependent, e.g., due to dust or atomic scattering:

$$p_{obs} \sim p_{max}(\lambda)g(\Theta,\lambda)\tau_s(\lambda). \quad (4.7)$$

However, this is ruled out for hot stars, due to the "grey" Thomson-scattering process.

According to Brown & McLean (1977) [9], an axisymmetric scattering envelope leads to

$$p_{obs} \sim \tau_s(1-3\gamma)\sin^2 i, \quad (4.8)$$

where γ is an envelope shape factor (for a spherical envelope $\gamma = 1/3$; $\gamma = 0$ (1) for a flat (oblate) disk), i is the inclination, and $\tau_s = \sigma_T \int_V N_e(R)dV$, with the electron density distribution $N_e(R)$. The Thomson-scattering cross section is wavelength independent and the scattering process does not alter the scattered spectrum.

Chandrasekhar suggested that the best condition for observable polarization from the limbs of early-type stars should be the symmetry breaking effect of the eclipse by a companion. This phenomenon has been reported by Robert et al. (1990) [59] and extended by St-Louis et al (1993) [79] for the WR binary V444 Cygni.

Schulte-Ladbeck et al. gave an example for wavelength dependence (cf. Fig. 4.4) for the WR star EZ CMa.

To consider the different aspects of wavelength dependence she split the WR star into three different zones: a *continuum-forming region*, a *line-emitting region*, and an *electron-scattering region*. If we suppose that the scattering events happen close to the star, whereas the emission line forming region is at large distances, then

the line polarization is almost zero; recombination emission is unpolarized and the radiation is emitted far from the scattering electrons. The result is a reduced level of polarization in the emission lines. Because of this *dilution effect* it is necessary to treat the continuum and line forming regions *together* with the scattering regions.

Figure 4.5 presents a sketch of a radiatively driven WR wind with an equatorial material enhancement. If different lines are formed in different radii (this is a reasonable assumption, as we will see later), then they will also show different amounts of polarization. The geometry of the continuum and line scattering regions is the same and their co-linear polarization vectors lie perpendicular to the equatorial plane. In the Q-U diagram of Fig. 4.5, the polarization at different wavelengths will follow a straight line. This is valid for the continuum as well as for the lines if there is no interstellar polarization component. The correction for interstellar polarization is possible with the "Serkowski law" (Serkowski et al., 1975 [73]), which gives the shape of the interstellar polarization as a function of wavelength.

A common problem in observations of intrinsic polarization is that of small contrast. Assuming an interstellar polarization of 1% and an intrinsic stellar polarization of about 0.1% with a flux-to-continuum ratio in the line of 10, then the continuum polarization is 1.1% and the line polarization is 1.01%. For a 3σ detection of this feature we need an internal accuracy of at least 0.03% per pixel. This means that a signal-to-noise ratio of 3000(!) is necessary. So, to observe not only bright but also faint stars and to understand the nature of variability we need a large telescope for a reasonably long run.

(B) Time-dependence

As an example Figure 4.6 shows the sketch of a star with a radiatively driven wind containing clumps at random time intervals in an equatorial plane with an axisymmetric distribution. Integrated over the ensemble of clumps at any time, the direction of the polarization vector is more or less constant with time. If plotted in a Stokes-Q-U diagram the data points for different clumps lie along a line. Each data point represents the vectorial sum of a time independent interstellar polarization vector and the intrinsic polarization vector with temporal variations. The polarization position angle Θ will remain constant, due to the geometry. If the interstellar polarization is known, we could estimate the true zero point for the intrinsic coordinate system and hence the direction on the plane of the sky in which the material is concentrated.

To obtain the shape of the data points in the Q-U plane and thus to answer the question if there is a special wind geometry *and* variability, many observations are necessary.

(a) In the case of *random* variability one *always* observes the preferred axis, but not vice versa. The preferred axis is always visible in the Q-U plane.

(b) There will be a certain number of disk-like systems which exhibit random variability because they are seen nearly pole-on. For such systems we can detect random but not a preferred direction of variability.

(c) If the atmosphere shows no temporal variability, this only means that the wind is homogeneous; its geometry would remain unknown. A steady-state disk would not show polarization variations.

4.3 Intrinsic circular polarization

The creation of linearly polarized light is also possible via cyclotron emission. As mentioned in 2.2 an electron captured by a magnetic field spins around the field lines and emits Bremsstrahlung which is polarized. The emitted wave oscillates perpendicularly to the field direction. In the direction of the field the electrons emit circularly polarized light. One refers to a transverse and a longitudinal field for the field components perpendicular and parallel to the observer's direction, respectively. This means that if we see circularly (linearly) polarized light, we look "onto" the electrons with their spin parallel (perpendicular) to the line-of-sight. As a result, circularly polarized light is a relatively unambigous indicator for intrinsic magnetic fields. Linearly polarized light is an indicator of scattering processes as well as magnetic fields.

The detection of magnetic fields is done through the observation of the Zeeman effect in spectral lines. The energy levels of an atom in an external magnetic field are split into 2J + 1 sublevels. The energy difference of these sublevels is $\Delta E = gehB/4\pi mc$, were g is the Landé factor. As a result, the atomic lines are also split and we call the components for which $\Delta M = \pm 1$ (quantum number M for angular momentum) the σ component and for $\Delta M = 0$ we call them the π components. These components are polarized: For a transverse field, the π components are linearly polarized parallel to the field and σ components are polarized perpendicular to it. For a longitudinal field the σ components have opposite circular polarizations, whereas the π components are not visible. This situation is represented in Fig. 4.7 from Landstreet (1979 [34]) who published a review about magnetic fields in stars.

The differences between the analyzed line profiles in panel (c) of Fig. 4.7 are the basis for the detection of fields which are too weak to distort the profiles in (b). Figure 4.7 represents an ideal case of clearly separated longitudinal and transverse fields. The real case is, in general, more complex. As an example, Fig. 4.8 shows the effect of changing the field orientation with time.

In his paper Landstreet discussed several techniques of field measurements: *photographic Zeeman polarimetry*, *spectroscopy of stars with resolved Zeeman structure*, *photoelectric spectropolarimetry of metallic lines*, *Balmer-line Zeeman analyzer* and the *transverse Zeeman effect*. In addition, Landstreet also discusses the limitations of various methods of measuring longitudinal fields. An interesting effect arises when there is a patchy distribution of material. In that case, elements appear to be nonuniformly distributed on the stellar surface and the measured effective field is different for

different elements.

The geometries of magnetic fields can be very complex. Models are calculated for a centered dipole, a decentered one, a symmetric rotator, or a more complex one. A list of well determined geometries in several stars is given in Landstreet (1979) [34].

In the last few years the technique of Doppler imaging (the estimation of surface structures of an unresolved star using the Doppler effect) has made large advances. It is also possible to derive surface information about the distribution of magnetic fields with the technique of Zeeman Doppler imaging. This can be done with circularly polarized light. A description of this technique, the basic principles, numerical simulations and technical considerations are given in three publications by Semel (1989 [61]), Donati et al. (1989 [18]) and Semel et al. (1993 [62]).

The basic principles of the analysis of polarimetric measurements are given in the first paper by Semel (1989 [61]). If we assume a stellar disk, affected by two magnetc spots of opposite polarities, with no relative velocity to the observer, the sum of their circular polarizations would be reduced or cancelled out (see Fig. 4.9). In the case of non-zero stellar rotation, the relative velocities of the spots are separated due to the effect of circular polarization. Then,

- the measured global magnetic flux is reduced and differential measurements may lead to the determination of the line-of-sight component of the magnetic field, and
- to increase the S/N of Stokes V, one may add the signals from several lines, to increase the quality of magnetic field measurements.

From the technical point of view, the application of Zeeman Doppler imaging has some important requirements. (A) Because of polarization rates of the order of 0.1 percent, the S/N ratio must be high. (B) To see small scale structures the spectral resolution should be reasonably high. (C) Spurious polarization levels should be reduced to the level of the photon noise.

Semel et al. describe the double beam method with a $\lambda/4$ plate and a beam splitter in their publication and its problems due to wavelength dependent differences between the two intensities of the orthogonal states of polarization:

(A) Time dependent effects

1. Doppler shifts between two observations due to radial velocity variations of stellar or terrestial origin.
2. Stellar rotation or variability which may cause some spectral changes.
3. Drift in the spectrograph.
4. Variations of the star image (projected onto the slit) between successive exposures.

(B) Effects in the double beam set-up.

In the case that two beams are measured on different CCD columns.

1. The sensitivity calibration of the detector pixels is not known to the precision better then 10^{-3}.
2. Aberrations in the optics may make the two spectra slightly different.
3. Misalignment of the detector may cause small wavelength differences between the corresponding pixels of the two spectra.

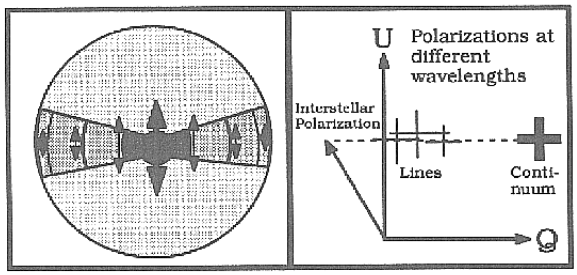

Figure 4.5: Cartoon depicting a steady-state "disk". The continuum polarization has a direction perpendicular to the disk. Lines formed at increasing radii exhibit decreasing amounts of polarization, but the direction of the line polarization is the same as the continuum polarization. Thus, at a given time, polarizations measured in the continuum and different lines lie along a straight line in the Q-U plane. (Schulte-Ladbeck et al., 1992).

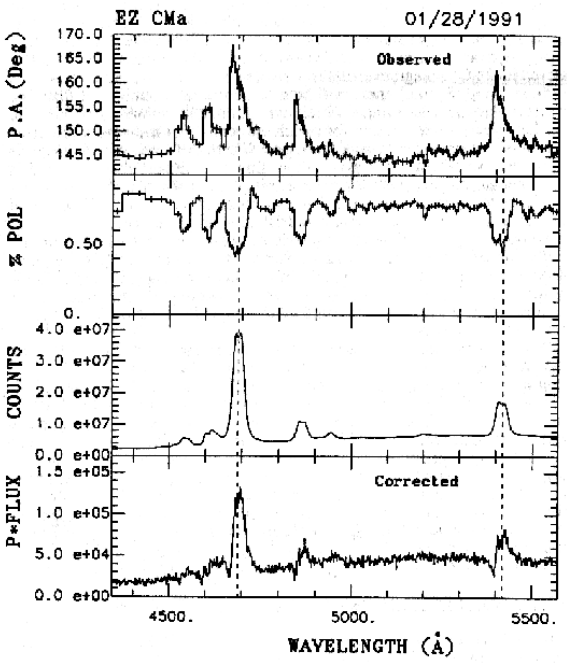

Figure 4.4: Total counts, polarization in percent, and position angle in degree versus wavelength for EZ CMa, measured at the AAT. Error bars are $\pm 1\sigma$. Changes across line profiles, which are different in flux and polarization, can be seen. P*FLUX is the spectrum of the polarized counts after correction for interstellar polarization. Dashed lines mark the positions of the observed line centers for HeII 4686 Å and 5412 Å in the count spectrum. (Schulte-Ladbeck et al., 1992).

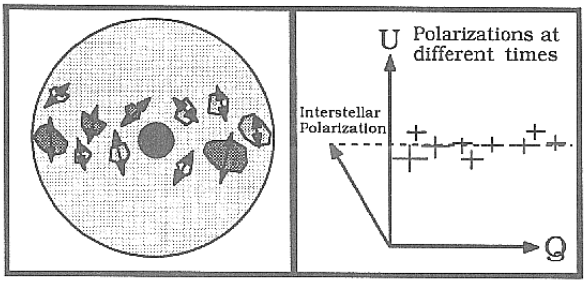

Figure 4.6: Polarization from axisymmetric "clumps". When the polarization is measured at different times in a continuum filter, individual data points are found to fall along a line in the Q-U plane, because the spatial distribution of the clumps has a preferred plane, and thus there exists a preferred direction of the polarization (Schulte-Ladbeck et al., 1992).

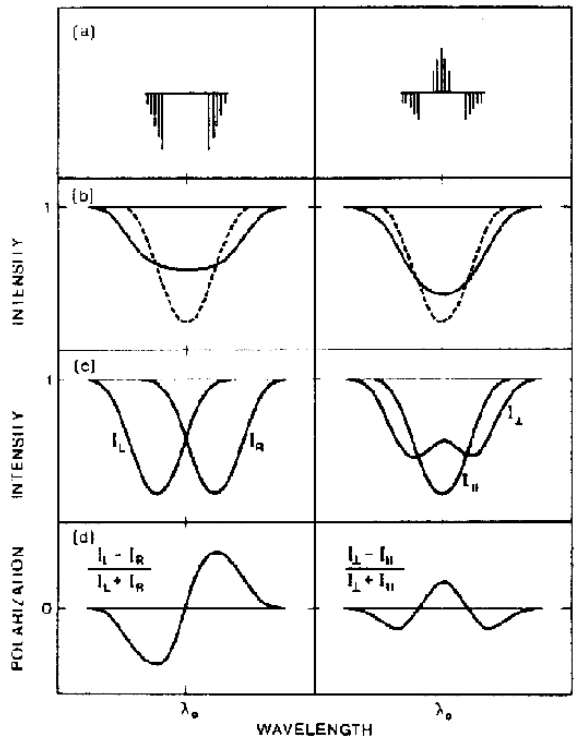

Figure 4.7: Wavelength dependence of emergent intensity and polarization across a spectral line split by a longitudinal (left) and a transverse (right) magnetic field. (a) The splitting of a spectral line for a $^3P_2 - ^3D_3$ transition, π components above the line and σ components below, with the lengths of the bars indicating the strengths; (b) The appearence of the stellar absorption line with a field present (solid) and absent (dashed); (c) On the left side: the line profile as seen in right (I_R) and left (I_L) circularly polarized light; (c) On the right side: the line profile seen in linearly polarized light parallel ($I_\parallel$) and perpendicular ($I_\perp$) to the field. (d) The net circular polarization (left)($V = (I_L - I_R)/(I_L + I_R)$) and linear polarization (right) ($Q = (I_\perp - I_\parallel)/(I_\perp + I_\parallel)$) across the line (Landstreet, 1979)

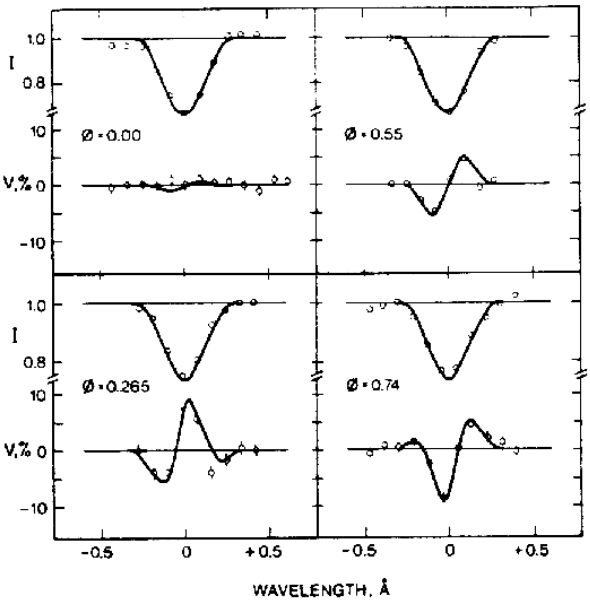

Figure 4.8: Flux and circular polarization profiles of Fe II 4520.2 Å in 78 Vir at several phases. The points are observed data, while the smooth curves are the predictions of the model, given in Landstreet (1979). The profiles clearly show the added complexity which arises from the rotational broadening of the line.

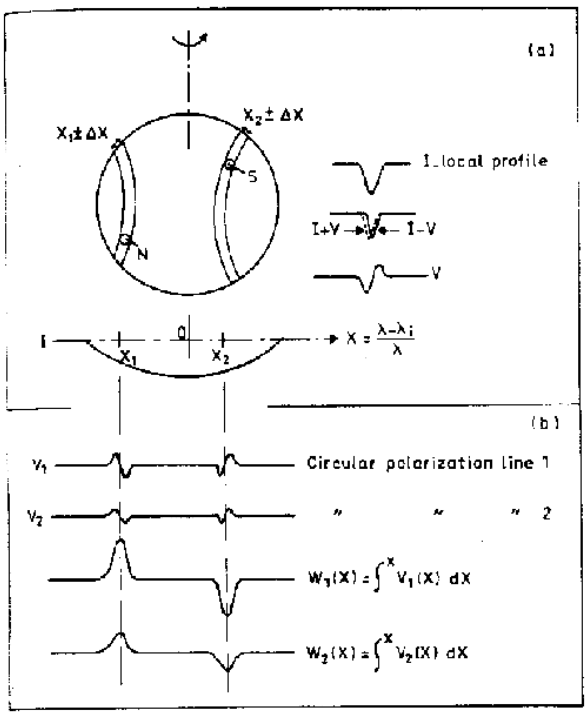

Figure 4.9: The star can be divided into zones of equal velocity. The light emerging from each zone has a particular Doppler shift. In the spectrum, the contributions from different zones to a given spectral line are separated by their Doppler shift. Circular polarization due to the first magnetic spot appears at X_1, and the second at X_2 in the V profiles. The same is true for all spectral lines. **(a)** On the right, the two profiles $I + V$ and $I - V$ correspond to the two states of circular polarization. Their difference gives Stokes V. It has a particular shape easy to recognize. Each stellar spot contributes such a signal to the spectrum at the appropriate wavelength. **(b)** The observed circular polarization in the stellar spectrum. V_1 and V_2 correspond to the lines 1 and 2 respectively. W_1 and W_2 are the integrals of V_1 and V_2 respectively (Semel, 1989).

Chapter 5

Spectropolarimetry of hot stars

According to the classical MK spectral classification system, the A, B and O stars represent the group of hot or early type stars. Wolf-Rayet stars with their strong spectral *emission* lines belong also to this group. I discuss here what is known about each type in the context of spectropolarimetry.

5.1 B and A stars

With temperatures of about 25 000 K - 10 000 K (B0 - B9 type) and 10 000 K - 7500 K (A0 - A9 type), **B and A stars** are those with the lowest surface temperatures in the group of early-type stars. They exibit outmoving atmospheres in the form of stellar winds, driven by their radiation field. Wind velocities and mass loss rates are generally much inferior to those of O or Wolf-Rayet stars but are still significant.

For a long time it was generally assumed that the winds of early-type supergiants are spherically symmetric. Meanwhile the common view is that they are rather inhomogeneous and asymmetric, in general.

Taylor (1992) [82] presented optical spectropolarimetry of the B1Ia stars κ Cas and P Cygni. The data were obtained between 1989 and 1991 at Pine Bluff Observatory, extended to the UV by the Wisconsin Ultraviolet Photo-Polarimeter Experiment (WUPPE), the first orbiting spectropolarimeter. For κ Cas she reported a variability in polarization (ΔP) of 0.18% which is lower than previously determined variations. Hayes (1984) [27] detected variations of 0.38% in 1976 and 1978, whereas Lupie & Nordsieck (1987) [37] measured 0.27% in 1981 and 1982.

Taylor suggested that this reduced variability may indicate that the material surrounding κ Cas is becoming more spherical with time.

The intrinsic polarization of P Cygni varied by 0.59% while the position angle changed between 2° and 179° indicating that the scattering material is randomly placed around the star. It is clear from these data, that the distribution of circumstellar material is not spherically symmetric. Time-dependent localized regions of enhanced electron density are perhaps embedded in a spherically symmetric global wind. These density enhanced regions propagate outwards, $\int n_e^2 dV$ becomes smaller, and the shape of the polarization curve becomes flatter with time. The wavelength dependence of the position angle in her data suggests that multiple "blobs" may always exist in the wind.

5.2 Be stars

A very remarkable group under the B types are the **Be stars**. These stars of luminosity class III-V are believed to be fast rotators (Slettebak, 1976 [75]), so that a radial symmetric gravitation and radiation field cannot be assumed. They show strong stellar winds (Dachs, 1980 [17]), and narrow absorption components in their wind emission line features, indicating an equatorial thin disk of about 20 stellar radii extension between a latitude independent material outflow. Be stars show strong spectral variations over timescales from hours to years.

A fundamental problem in explaining Be stars is the coexistence of two totally different mechanisms: (a) The latitude independent radialsymmetric wind has typical temperatures of the order of 10^5 K, with velocities of the order of 1000 – 2000 km/s, whereas (b) the equatorial disc shows temperatures of the order of 10^4 K with no outflow (see e.g., Fig. 5.1 and Hanuschik, 1996 [23]).

After several efforts to explain as many phenomena as possible (e.g., Rotation Model by Struve (1931) [81], NRP Model by Baade (1984) [2], Elliptical Ring Model by Huang (1974 [31])), a general explanation for the creation of an equatorial disk has been given recently by the self-consistent Wind Compressed Disk (WCD) Model of Bjorkman & Cassinelli (1993) [7]. This has been supported by Owocki, Cranmer & Blondin (1994), who explain the steady-state behavior of the disk with hydrodynamical simulations. The fundamental parameter of the WCD model is a threshold of the rotational velocity V_{rot} for creating an equatorial disk, relative to a wind terminal velocity V_∞.

Because of this global deviation from radial symmetry, Be stars are strong candidates for the detection of linear polarized light due to electron scattering. From the variability of the polarization level and its wavelength dependence, we can investigate changes in the disks of Be stars. Polarization (including line effects) serves as a probe of both the physical properties (density, temperature and composition) and the geometry (distribution of matter). The first polarimetric observations of a Be star were made by Behr (1959) [5] for γ Cas, with an indication of intrinsic variations. A polarimetric survey of several Be stars was presented by

Clarke & McLean (1974) [15] and observations of γ Cas by Poeckert & Marlborough (1977 [54], 1978 [55]).

The first spectropolarimetric observation of a Be star was made by Poeckert & Marlborough (1977) [54]. They detected linear polarization across the Hα line in γ Cas using the Poeckels cell polarimeter at the University of Western Ontario 1.2m telescope. They also presented model calculations which indicate that changes of the polarization position-angle are due to the disk-like envelope surrounding the Be star.

The observational results of Poeckert & Marlborough were qualitatively confirmed (depolarization in the lines, changes of the position angle) two years later by McLean et al. (1979) [44]. They obtained linear polarization of Hβ for the four shell stars γ Cas, ϕ Per, ψ Per and ζ Tau with a 106 element Digicon spectropolarimeter. In their configuration they recorded a spectral range of 32 Å. For ψ Per Figure 5.1 shows the normalized intensity I, the polarization P in percent, and the position-

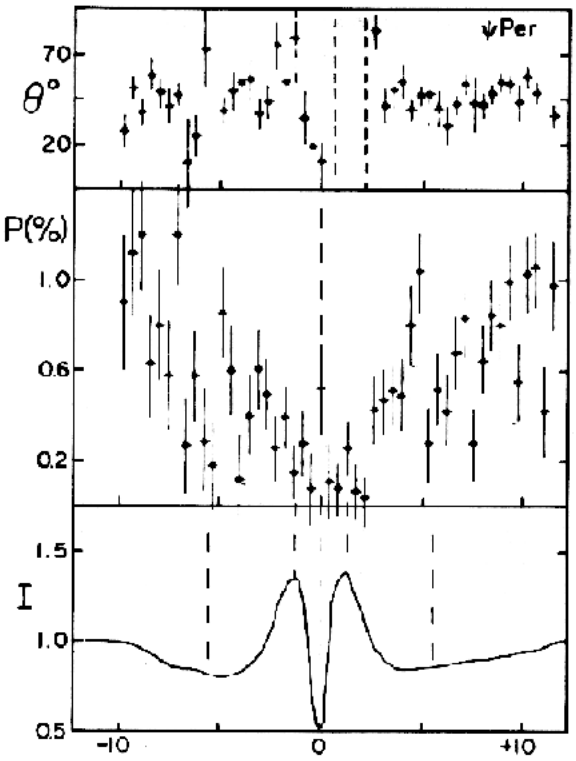

Figure 5.1: Flux and linear polarization across Hβ (Å from centre) for ψ Per. The position angle Θ is relative to the equatorial system, polarization in percent. The error bars are $\pm 1\,\sigma$ (McLean et al., 1979).

the rotationally broadened Hβ line with a strong central disk-absorption is seen to decrease sharply towards line centre, following the onset of unpolarized emission flux, as expected (see 4.2). Note: One should compare the poor accuracy of these first data with those of Schulte-Ladbeck et al. (1992) [67] in Fig. 4.4 around 14 years later.

To visualize the separation between intrinsic and interstellar polarization, McLean et al. (1979) plotted the normalized Stokes parameters $p_x = p\cos 2\Theta$ versus $p_y = p\sin 2\Theta$ as a function of wavelength across the line. Because the interstellar polarization is expected to be constant over 30 Å, any deviation from a straight line in the $p_x - p_y$ plane (a loop here) should be due to intrinsic polarization. The sense of this loop is expected to be related with the sense of rotation of the star/envelope projected on the sky (Poeckert & Marlborough, 1978 [55] and McLean, 1978 [46]). Figure 5.2 shows their corresponding $p_x - p_y$ plot for ψ Per.

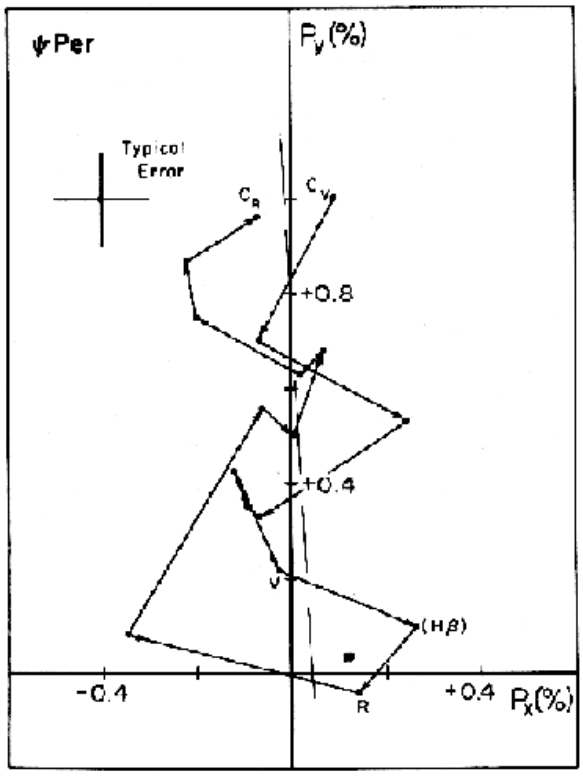

Figure 5.2: Corresponding Stokes parameter diagram for ψ Per. The points generated from the previous are averaged values over 1.35 Å intervals and are shown in uniform steps of 1.35 Å. Arrows indicate the direction of increasing wavelength and typical $\pm 1\sigma$ error bars are shown. The lightly drawn dashed line indicates the approximate mean direction of the intrinsic plane of polarization (McLean et al., 1979).

Because of its brightness γ Cas ($m_{vis} = 2.5\,mag$) is *the* standard target among all Be stars and with twice the resolution the same observation was made around 15 years later by Jiang et al. (1993) [33], who confirmed the behavior of the polarization over the line. They also found that the polarization profile is much wider than that of the emission line flux. In addition, they modeled the Hβ profile of the underlying star. They found that linear polarization profiles across emission lines are not only affected by the emission from the disk, but also by

the profile of the underlying stellar absorption feature. Thus, the observed profile of linear polarization must be also contain information about the central star.

Bjorkman (1992) [8] observed the Be star π Aqr over a time interval of two years at Pine Bluff Observatory between 3200 Å and 7600 Å. The comparison of the time dependent behavior of the Hα equivalent width and the mean polarization is seen in Fig.5.3. It seems that

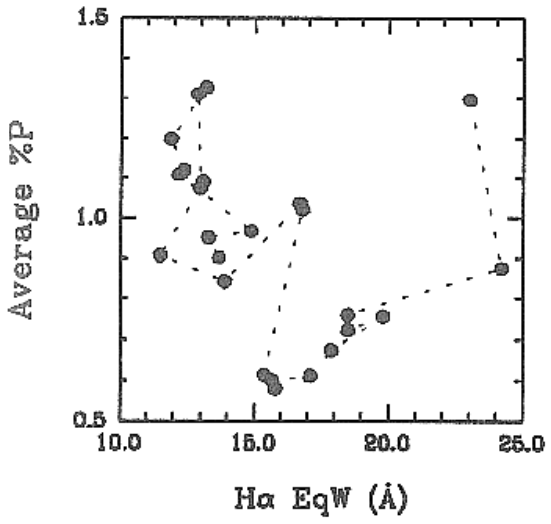

Figure 5.3: Average polarization and Hα equivalent width of π Aqr plotted as a function of time (Bjorkman, 1992).

changes of the polarization are correlated with changes in Hα equivalent width but there is no indication of a correlation between the sign (i.e. increase or decrease) of the polarization change and the sign of the change of the Hα equivalent width. Figure 5.4 shows the behaviour of π Aqr in the Q-U plane. Each data point gives the values of Stokes Q and U of an observation during two years. As expected (see section 4.5), the data for π Aqr, with a known equatorial disk, lie on a straight line which gives also the position angle of the polarization on the sky.

In a search for magnetic fields in Be stars via the Zeeman effect in the wings of Hβ, Barker et al. (1985 [4]) could not detect any longitudinal magnetic field in a sample of 15 Be stars. Nevertheless, large surface fields can escape detection because of geometry and orientation. This is explained in 5.4.

5.3 Bp and Ap stars

Ap stars (Si or Sr-Cr-Eu) and He-weak or He-rich Bp stars are the only upper-main sequence stars which exhibit well-established magnetic fields. This fact makes them standard targets for circular polarization observations. Typical observed longitudinal field strengths range from 3×10^2 G to 2×10^4 G.

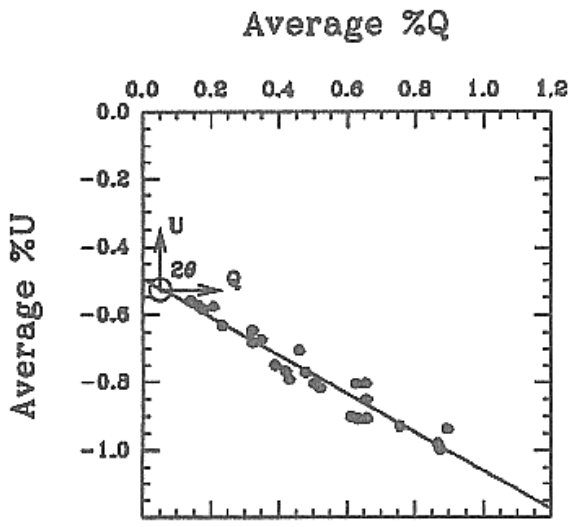

Figure 5.4: Q-U diagram for π Aqr (Bjorkman, 1992).

Observations of peculiar A and B stars have been made in linear as well as circular polarized light. As an example for spectropolarimetric observations in the Stokes V parameter, an important series of five papers about spectropolarimetry of upper main sequence peculiar (CP) stars are considered:

Spectropolarimetry of magnetic stars;

I. Diagnostic contents of Stokes I and V line profiles (Mathys & Stenflo, 1986 [39]).

II. The mean longitudinal field (Mathys, 1991 [40]).

III. Measurement uncertainties (Mathys, 1994 [41]).

IV. The crossover effect (Mathys, 1995 [42]).

V. The mean quadratic magnetic field (Mathys, 1995 [43]).

The bases of these papers arises from simultaneous observations of Stokes I and V in 16 lines of Fe II and five lines of Si II, carried out with the Cassegrain Echelle Spectrograph (CASPEC) at the ESO 3.6m telescope.

Including a description of CASPEC, the first publication (paper I) describes the I and V line profiles in terms of simple parameters and investigates mutual dependences on, and correlations with, atomic parameters over a spectral range of about 1000 Å with a resolving power of 20 000. The sample target was the late Bp (Si-Cr-Sr) star HD 147010 with a well known, large longitudinal field of ~ 5 kG.

The mean longitudinal magnetic fields (also often called the effective magnetic field) $\langle H_z \rangle$ of the stars are determined by using the "photographic technic" (paper II). The wavelength shift of lines between spectra simultaneously recorded in right and left circular polarization is interpreted in terms of the mean longitudinal magnetic field $\langle H_z \rangle$:

$$\lambda_R - \lambda_L = 2\bar{g}\Delta\lambda_Z\langle H_z\rangle. \quad (5.1)$$

λ_R and λ_L are the wavelengths of the centre of gravity of the line in right and left circular polarized light, respectively:

$$\lambda_R = \frac{1}{W_\lambda}\int r_{\mathcal{F}_R}(\lambda)\lambda d\lambda. \quad (5.2)$$

W_λ is the line equivalent width, $r_{\mathcal{F}_R}(\lambda)$ is the relative line depression in right circularly polarized line, $\bar{g}$ is the effective Landé factor of the transition, and $\Delta\lambda_Z = k\lambda_0^2$ is the Lorentz unit with λ_0 as the rest wavelength of the transition and $k = 4.67\times10^{-13}\text{Å}^{-1}\text{G}^{-1}$. The mean longitudinal field derived from this application is the line-intensity weighted average over the visible stellar disk:

$$\begin{aligned}\langle H_z\rangle &= \frac{1}{W_\lambda\mathcal{F}_{I_c}}\int_0^{2\pi}d\phi\int_0^{\pi/2}H_z\cos\Theta\sin\Theta\ d\Theta \\ &\times \int[I_c - I(\lambda)]d\lambda. \quad (5.3)\end{aligned}$$

Here $\mathcal{F}_{I_c}$ is the flux in the continuum at the line wavelength, ϕ and Θ are the coordinates on the stellar surface, I_c and $I(\lambda)$ are, respectively, the local intensity in the continuum and in the line, at the point (Θ,ϕ).

With these tools, Mathys determined longitudinal fields for a sample of 30 Ap stars with an accuracy of ~ 80 G in the best cases.

Discussing the measurement uncertainties (paper III) via statistical methods he then measured the *Crossover Effect* in his paper IV. This effect appears close to the phases when the mean longitudinal field reverses its sign, or "crosses over" from one polarity to the other. An illustration is given in Fig. 5.5.

One can see that

1. the lines look rather alike in both polarizations at phase 0.753, close to the longitudinal field negative extremum.
2. they are systematically sharper in right circular polarization than in the left one at phase 0.011, close to the positive crossover of $\langle H_z\rangle$, and
3. they are consistently broader in right circular polarization than in the left one at phase 0.514, close to the negative crossover.

The nth-order moment of a line profile recorded in Stokes V with respect to the wavelength λ_0 of the center of gravity of the corresponding unpolarized profile is defined as

$$R_V^{(n)}(\lambda_0) \equiv \frac{1}{W_\lambda}\int r_{f_v}(\lambda-\lambda_0)(\lambda-\lambda_0)^n d\lambda, \quad (5.4)$$

were W_λ is the (unpolarized) equivalent width of the line and r_{f_v} is the line profile in the Stokes V parameter $r_{f_v} \equiv (f_{V_c} - f_V)/f_{I_c}$. f_V is the flux in Stokes V in the line and f_{V_c} that of the neighbouring continuum. f_{I_c} is the unpolarized flux in the neighbouring continuum.

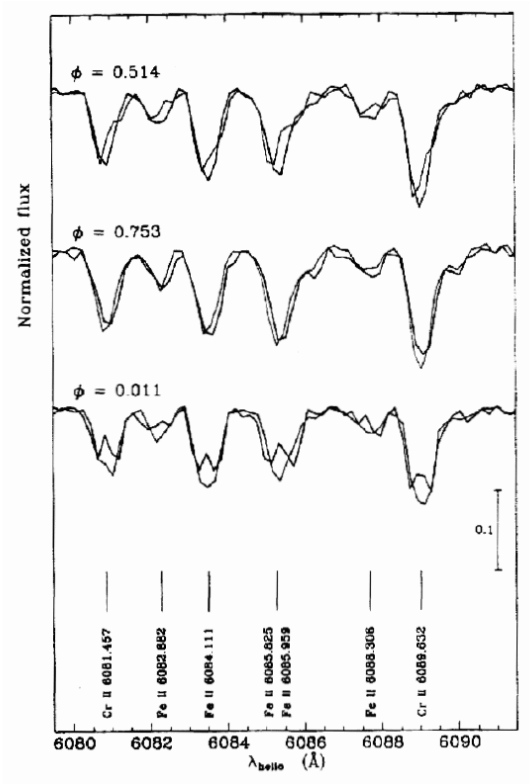

Figure 5.5: Portion of the spectrum of HD 153882 recorded in right (thin line) and left (thick line) circular polarization at three phases (Mathys, 1995).

Following this expression, he expressed the second-order moment.

$$R_I^{(2)} = C + [(C_2^{(1)} + C_2^{(0)}) + \alpha(C_2^{(1)} - C_2^{(0)})]\Delta\lambda_Z^2\langle H^2\rangle. \quad (5.5)$$

$\langle H^2\rangle$ is the square of the magnetic field modulus, integrated over the visible stellar disk, $C_2^{(1)}$ and $C_2^{(0)}$ are quantities characterizing in a global manner the Zeeman pattern of the considered transition, α is a parameter, comprised between 0 and 1, and C is a constant. With these expressions Mathys describes the crossover effect in terms of the *second order moment* of the Stokes V line profiles. He shows that one can derive from these measurements a quantity called the mean asymmetry of the longitudinal magnetic field, which is the first moment of the component of the magnetic field along the line-of-sight, about the plane defined by the line-of-sight and the stellar rotation axis.

Finally, he measured the mean quadratic magnetic field (paper V), which is the square root of the sum of the mean square magnetic field modulus and of the mean square longitudinal magnetic field $\sqrt{\langle H^2\rangle + \langle H_z^2\rangle}$ (the square root is used to have the more useful dimension of a magnetic field). The lower limit of detection of quadratic fields was of the order 5 kG and the observed quadratic fields range from 5 kG to 37 kG.

Table 5.1: Surface brightness weighted average of longitudinal field strengths and standard deviation (Barker et al., 1981).

JD 2,444,300+	B_e (gauss)	σ (gauss)
27.83	-110	138
48.62	-71	113
50.58	+48	65

5.4 O stars

The most permanent luminous stellar objects are the **O stars**. They exhibit strong, fast stellar winds of relatively low opacity, driven by their strong radiation field. Luminosities are found to be up to $10^6 L_\odot$ (for O supergiants) with mass loss rates $\dot{M}$ of up to 5 $\times 10^{-6} M_\odot$. Terminal wind velocities (V_∞) of up to 2000 km/s are found. Estimated surface temperatures are found to lie up to $\sim$ 50 000 K. In an evolutionary context, O stars are the probable progenitors of Wolf-Rayet stars (see 5.5).

Because of its brightness, ζ Puppis is the most observed O star, and this will not change for polarimetry, of course. In order to search for a magnetic field, Barker et al. (1981 [3]) tried to measure the longitudinal Zeeman effect in the wings of Hβ of ζ Puppis, with a photoelectric Pockels cell polarimeter. Their values of the mean longitudinal detected field are given in Table 5.1.

From these results only, one cannot conclude, that a magnetic field is really present. Nevertheless, Barker et al. argue that there *may* be much higher field values, which are possibly not detectable because of an unfavorable combination of field geometry and stellar orientation. If a $v \sin i$ of 210km/s, given in earlier publications, is correct, ζ Puppis is seen almost equator-on. For this orientation, possible field geometries are given in Fig. 5.6.

Using the expressions derived by Schwarzschild (1950 [69]) the centered dipole field with the dipole axis parallel to the rotation axis (case A) yield no longitudinal field measurements ($B_e = 0$), independently of the field strength B_p at the pole. With an inclination $i = 70^\circ$ it is possible to have $B_p \approx 1kG$ with $B_e \leq 100$ G.

Case B is common among the known magnetic stars: a centered dipole with axis in the rotational equatorial plane. B_e will vary sinusodially and an observed $B_e \leq$ 100 G implies a $B_p \leq 300$ G. Barker et al. could not exclude this possibility for ζ Pup because of incomplete phase coverage.

A quadrupole geometry with an alignment of the field axis with the rotation axis (case C) with a $B_e \leq 100$ G implies a $B_p \leq$ 2–4 kG. But no stars with predominantly quadrupole fields are known among the chemically peculiar stars, and so they conclude, that it is not clear how plausible a pure quadrupole model of ζ Pup might be.

Linear spectropolarimetry at high signal-to-noise ratio for the Hα line of ζ Pup was presented by Harries & Howarth (1996 [25]; see also [24]). Their polarization measurements are given in Table 5.2, which lists the measured polarization in three bins; one 4-Å bin at the line centre (6563 Å, one in the maximum of the line emission at 6568 Å, and one over a line-free continuum region at 6760 - 6860 Å. The plots of the Hα polarization spectra of ζ Pup for three consecutive nights are given in Fig. 5.7.

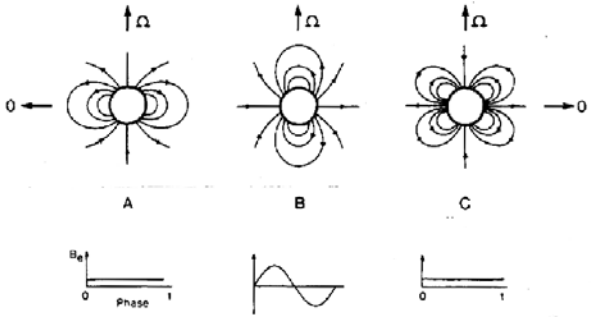

Figure 5.6: Three possible magnetic field geometries for a rotating star with a magnetic field, measured during a rotation period by an observer whose line-of-sight lies near the equatorial plane 00. (a) Centered dipole with rotation and magnetic axes parallel. (b) Centered dipole with rotation and magnetic axes orthogonal. (c) Linear quadrupole with an axisymmetric purely radial field in the equatorial plane (Barker et al., 1981).

Table 5.2: Polarization measurements from 3 observations. The statistical error on the line centre and maximum emission measurements are 0.008% while the error in the continuum is 0.002% (Harries & Howarth, 1996).

Date Mar. 1992	Line centre $\bar{q}$ (%)	Line centre $\bar{u}$ (%)	Emission $\bar{q}$ (%)	Emission $\bar{u}$ (%)	Continuum $\bar{q}$ (%)	Continuum $\bar{u}$ (%)
15^{th}	0.090	0.081	0.033	0.007	0.041	0.018
16^{th}	0.096	0.093	0.035	0.007	0.042	0.024
17^{th}	0.056	0.068	0.018	0.009	0.021	0.023

To establish the polarization enhancement they plotted the data in the $\bar{q}$ - $\bar{u}$ - plane with 3 σ errors (see Fig. 5.8).

One can see that the difference between the polarization of the line centre and the continuum is more than 4 σ. But nevertheless, this significance should be handled with care because of an instrumental correction due to reflections in the $\lambda/2$ plate.

Recent ultra-high signal-to-noise spectroscopic measurements of the HeII line of ζ Pup by Eversberg, Lépine & Moffat (1996) [21] show outmoving micro-structures in the strong O star wind. Assuming that these struc-

tures are generated by "blobs" one clearly can expect to detect linear polarization features.

5.5 Wolf-Rayet stars

Intense emission lines of various ionized elements are the spectral characteristics of **Wolf-Rayet stars**. Beals (1929) [6] realized that an extended, and rapidly expanding atmosphere is responsible for these features. Among all stable stars, WR stars reveal the strongest mass loss via wind mechanisms. Typical mass loss rates range from $(2-10)\times 10^{-5} M_{\odot}\, yr^{-1}$, with wind velocities of 1000 - 2500 km/s (Willis, 1991 [84]). The Wolf-Rayet winds are mostly opticaly thick, so the surface is not visible. This means that the connection of spectral classification to photospheric core temperature is not possible as for normal stars via MK classification, and the WR classification is purely spectroscopic. WR stars are highly luminous, evolved, hot, massive stars, in the final state of their nuclear He burning. WR stars create significant quantities of heavy elements and enrich the interstellar medium through mass-loss.

The evolutionary scenario of WR stars is still in discussion. But the idea of an O type progenitor is widely accepted. Chiosi & Meader (1986) [14] thought that WR stars are descendants of OB stars, Langer et al. (1994) [36] suggest for $M_{ZAMS} \geq 40 M_{\odot}$ the scenario O $\rightarrow$ Of $\rightarrow$ H-rich WN $\rightarrow$ LBV $\rightarrow$ H-poor WN $\rightarrow$ H-free WN $\rightarrow$ WC $\rightarrow$ SN, and Crowther et al. (1995)[16] predict O $\rightarrow$ Of $\rightarrow$ WNL+abs $\rightarrow$ WN7 $\rightarrow$ WC $\rightarrow$ SN.

The latest review about Wolf-Rayet stars and their winds is given by van der Hucht (1994) [83] and Hillier (1996 [29]), where also the so-called *momentum problem* is explained. We define the ratio η by:

$$\eta = \frac{\dot{M} V_{\infty}}{L/c} \equiv \frac{\text{Wind momentum}}{\text{Radiation momentum}} \qquad (5.6)$$

This number gives an indication of the efficiency at which radiation momentum is imparted to the gas. Single scattering delivers $\eta \leq 1$. Because $\eta \gg 1$ for many Wolf-Rayet stars, multiple scattering must play a role. This is probably no problem in a dense WR wind, so that Owocki et al. (1995 [53]) prefer to call this the opacity problem rather than the momentum problem. However, sufficient opacity has yet to be accounted for.

The high degree of ionization in their winds coupled with a clear stratification (Schulte-Ladbeck, Eenens & Davis, 1995 [68]), yield a large number of free electrons, which can scatter stellar light and polarize it. *Broadband* polarimetry has led to a large amount of information about WR stars. Here a group of eight papers, *"Polarization Variability among Wolf-Rayet Stars. I. - VIII."* by St.-Louis et al. (1987 [77]), Drissen et al., (1987) [19], St.-Louis et al. (1988) [78], Robert et al. (1989a) [57], Robert et al. (1989b) [58], Robert et al. (1990) [59], Drissen et al., (1992) [20], and Moffat & Piirola (1993) is noted.

Briefly summarized:

I. Results are considered for a complete sample of southern WC stars brighter than 9th magnitude. Binary modulation was found in polarization; less stochastic variability with faster winds; and it was suggest that "blobs" can be more easily detected in low velocity, turbulent winds.

II. This anticorrelation between stochastic polarization variability and wind velocity was confirmed by the study of the six brightest southern WN stars. No binary modulation was found in the known, long-period WN7 + O binary HD 92740, as in the suspected WN8 + c (c = compact companion) binaries HD 86161 and HD 96548.

III. A new way to derive mass-loss rates of WR stars in binaries was proposed. The estimation of the inclination of the system via polarization measurements led to a correlation between $\dot{M}$ and the mass of the WR star.

IV. Circular polarization in the continuum emission of WR stars above an instrumental level of $\sigma_V \sim 0.01\%$ was not detected.

V. Confirming the anticorrelation between stochastic polarization variability and wind velocity for seven of the eight bright Cygnus WR stars, they also developed two models to explain the origin of blobs.

VI. The orbital inclination of the WR + O binary V444 Cygni was determined to be $i = 78^{\circ}.5$, in agreement with other methods. Also, they confirmed the assumption of Chandrasekhar that strong polarization variations should be visible during the eclipse of the WR star by the O companion. The WR radius was predicted to be $\leq 4 R_{\odot}$. Note: An improved analytical model for the eclipsing WR + O binary V444 Cygni was presented later (St.Louis et al., 1993 [79]).

VII. Monitoring the three single WR stars WR14 (WC6), WR25 (WN7), and WR69 (WC9), they found no significant variation in WR14, but for the other two $\sigma \sim 0.06\%$, as expected for late-type WR stars.

VIII. Finally, observations of the two non-eclipsing WC + O binaries HD 97152 and HD 152270 show variation in the continuum but none in the strong emission-line complex of CIII/CIV + HeII. They deduce that mainly light from the O companion scatters off electrons in a spherically symmetric wind and introduces modulated orbital polarization.

St.-Louis et al. (1995 [80]) observed EZ CMa with the IUE satellite in their IUE MEGA Campain during 16 consecutive days. The observed variations suggest a global wind structure pattern that remains quite stable in the frame of the star. It can best be explained by some kind of corotating interaction regions emanating from hot (magnetically?) active regions near the surface of the stellar core.

The first spectropolarimetric observation of a Wolf-Rayet star was made by McLean et al. (1979b [45]) for EZ CMa (WN5) with the same instrument as for their observations of Be stars (McLean et al., 1979a [44]) here in the range 3400 Å – 6000 Å with 48 Å resolution (for the HeII 4686 Å line they obtained 32 Å resolution). That EZ CMa shows strong variability is a well known fact (e.g., Robert et al., 1992 [60]). Serkowski (1970 [72]) found a deviation from spherical symmetry

from broadband polarization observations. The model of Cassinelli & Haisch (1974 [10]) then explained the observed polarization with a disk-like structure. A non-spherical atmosphere was established by McLean et al. due to varying degrees of linear polarization in HeI, HeII, NIII, NIV and NV lines, and from their data an edge-on view can be excluded. Figure 5.9 shows their observed relative flux I_R, polarization P in % and polarization angle Θ in degrees. Their plot of the data in the Q-U plane (Fig. 5.10) shows clearly that the intrinsic polarization over the spectrum is collinear, which implies a density enhanced disk-like structure in the atmosphere (see Schulte-Ladbeck et al., 1992 [67].

In the first two of a number of spectropolarimetry papers, Schulte-Ladbeck et al. (1990 [63] and 1991 [64]) published the discovery of linear polarization variations in the HeII wings of EZ CMa obtained at Pine Bluff Observatory in Wisconsin. Also for the first time, they detected polarization loops in the Q-U plane, like those seen in Be stars. This leads to the assumption that also in this WR star an axisymmetric, electron scattering envelope could be the reason for this behavior (Fig. 5.11). From their data they suggest a rotating and expanding disk-like density distribution around EZ CMa.

In their second paper, Schulte-Ladbeck et al. (1991 [64]) probe the wind structure of EZ CMa through electron distribution as measured by spectropolarimetry. They conclude that

1. the wind of EZ CMA is not spherically symmetric, because of a large amount of continuum polarization,
2. the polarization is due to electron scattering, since the continuum polarization spectrum is flat at most epochs,
3. the spectrum of continuum polarization may rise into the UV, which is due to frequency-dependent absorptive opacity in the helium continuum,
4. the continuum polarization has a large, quasi-static component which can be explained with an inclined-disk model. The disk extends rather far into the wind, because it is seen also in line-forming regions,
5. the preferred explanation for polarization variations is from density fluctuations in the wind,
6. line photons are electron scattered, since emission lines are polarized, although not as strong as continuum light,
7. ionization stratification is seen in this star.

Recent results of Morel et al. (1996 [48]) clearly show, that the intrinsic variations are not caused by a companion. EZ CMa seems to be a single star.

The impression that the continuum polarization rises into the UV was confirmed by the first linear polarization spectrum of EZ CMa and Θ Mus (WC6 + O9.5I) obtained in the region 1400 to 3200 Å by the Wisconsin Ultraviolet Photo-Polarimeter Experiment (WUPPE) (Schulte-Ladbeck et al., 1992b [66]). The continuum polarization, measured in several bands from around 1600 Å to 3100 Å, reached about 0.8%, which confirmed the picture of a distorted wind in EZ CMa. Although Θ Mus shows variability in polarized light of about 0.2% around a mean of 1.45% at 82° (St.-Louis et al., 1987 [77]), Schulte-Ladbeck et al. were able to fit their UV data with a Serkowski fit for the interstellar polarization. The position angle did not change from one emission line feature to another. They conclude that the intrinsic polarization of the Θ Mus system is not easily distinguished from interstellar polarization.

Observations in visible light for HD 191765 (WN6) showed similar results as for EZ CMa (Schulte-Ladbeck et al., 1992a [65]):

Strong wavelength-dependent continuum polarization, reduced polarization levels across emission lines, a general deviation from spherical symmetry, localized density changes, axisymmetric wind geometry and ionization stratification.

One of the most recent works about spectropolarimetry is the Ph.D. thesis of Harries (1995 [24]). Among others, he investigated 16 WR stars (mainly WN types but also 3 WC stars, single and binary) with state-of-the-art techniques and telescopes. Among these stars he found "line effects", polarization variability across their lines, in 4 single WN stars, 1 binary, and all 3 WC stars. For a few single stars, he supports the claim of non-spherical wind structure, either in an oblate form, axisymmetric ellipsoid or disk.

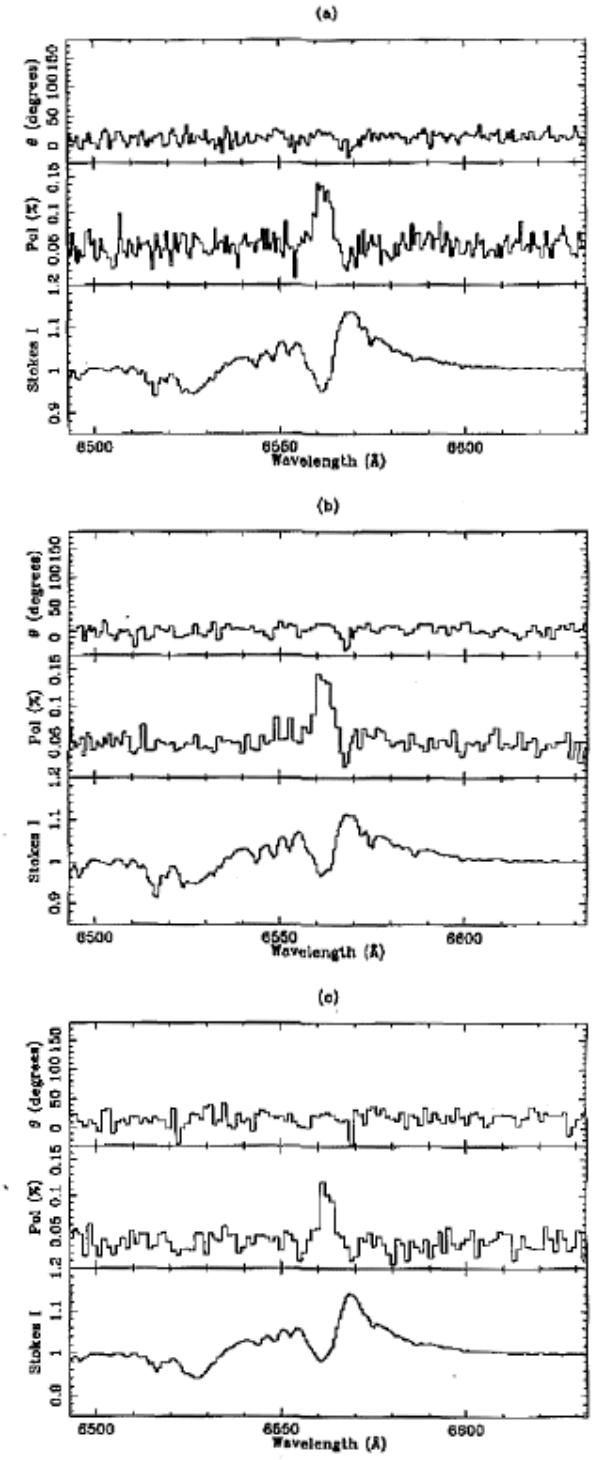

Figure 5.7: The Hα polarization spectra of ζ Pup; (a) 15th March, (b) 16th March and (c) 17th March 1992 (Harries & Howarth, 1996).

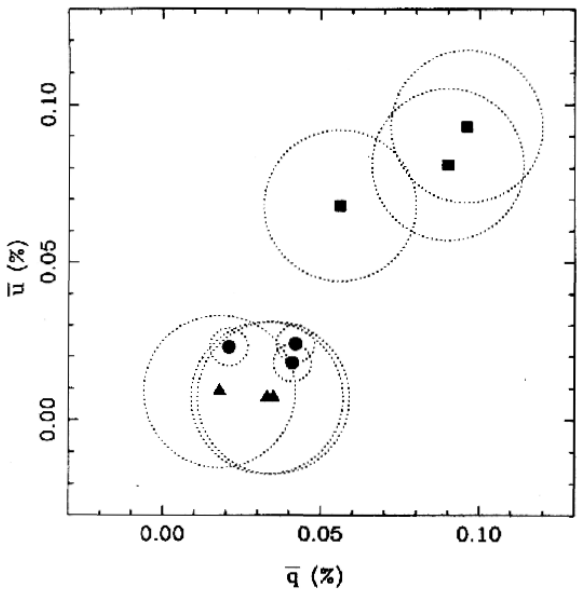

Figure 5.8: Q-U-diagram of the measured polarizations. The polarization of the enhancement (filled squares), the line centre (filled triangles) and the continuum (filled circles) are shown, along with their errors (dotted circles) (Harries & Howarth, 1996).

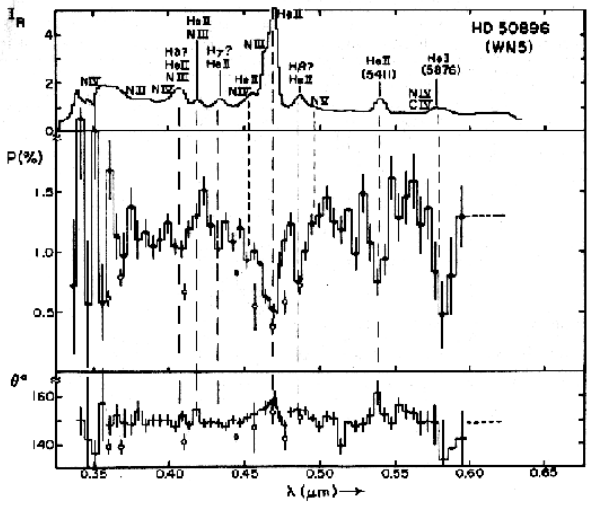

Figure 5.9: Relative flux, polarization and polarization angle of EZ CMa. Narrow band data obtained in Nov. 1978 are indicated with open circles. Error bars are $\pm 1\sigma$ (McLean et al, 1979).

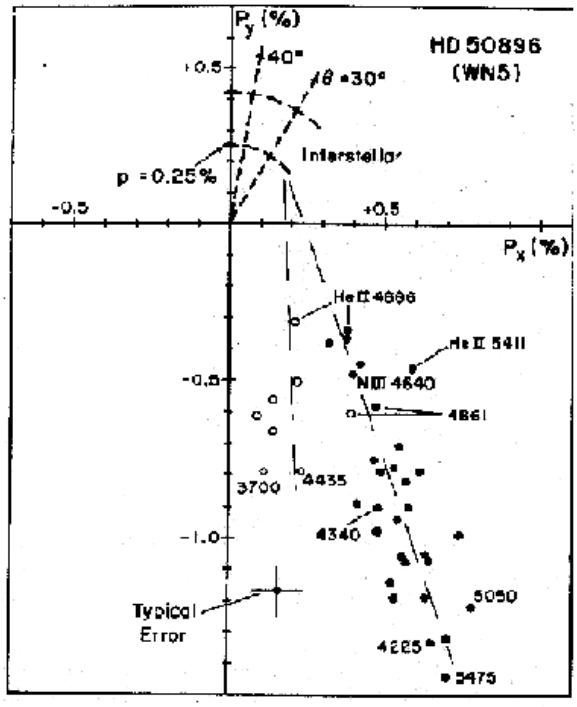

Figure 5.10: Polarization of EZ CMa in the wavelength region 4225 to 5475 Å. Open circles indicate data from 1978. Most likely interstellar values are also given (McLean et al., 1979).

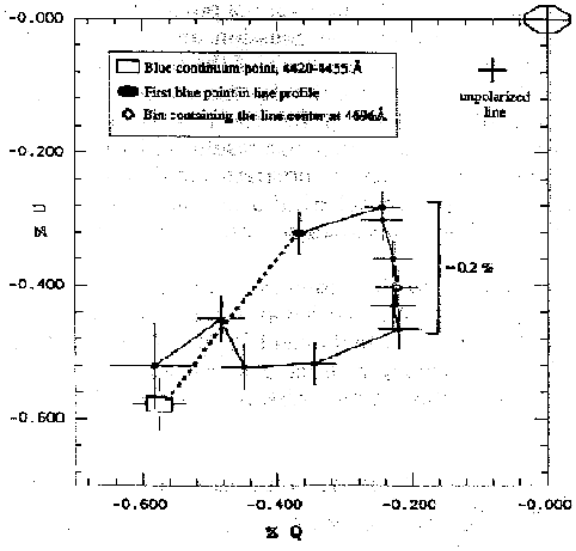

Figure 5.11: Interstellar corrected polarization data in Q and U for EZ CMa as a function of wavelength across the HeII 4686 Å line. The blue continuum, the first bin on the blue line and the line center are indicated by an open rectangle, a larger dot and by an open diamond, respectively. (Schulte-Ladbeck et al., 1990).

Chapter 6

Theoretical considerations

One of the biggest challenges in explaining the nature of hot stars is the modelling of their extended atmospheres. It is very clear that the analytical calculations are not only overwhelming in scope, but they just do not exist. The environmental conditions in hot stellar atmospheres are quite extreme. Electron temperatures of some 10^5 K with densities of $N_e \approx 10^{10-13} cm^{-3}$ led very early to the insight that the assumption of local thermal equilibrium (LTE) is not a good approximation for such conditions. The exponential term in the Boltzmann distribution is strongly dominated by the temperature and the energy transport is mainly carried by the radiation field of the star. We cannot deal with the Planck function but have to start with the general source function and, hence, the Saha equation is not usable.

Thus, analytical methods need many approximations for different parameters and exact results are not available. Nevertheless, a significant advance in developing numerical tools and methods has been made and moderate success in modelling stellar atmospheres has been achieved. One of the latest accomplishments was the first self-consistent model of a Be star and its equatorial disk by Bjorkman & Cassinelli (1993 [7]). The fundamental model parameter here is the fast rotation of the star (Be stars are rapid rotators) relative to the stellar wind velocity. The question arises, whether this is applicable to other types of stars too. Although disks in hot star types other than Be's is not seen, hot stars could, nevertheless, show density enhancements above the equator. Ignace et al. (1996 [32]) investigated the wind compression for a WN 5, a B[e] and an AGB star in a recent paper with the idea of a wind compressed zone (WCZ) over the equator. For the WR star, for instance, they found that a rotation of 16% of critical velocity leads to a density enhancement of a factor 18.5(!) with a reasonable, shallow wind ($\beta = 3$). From this point of view, we can expect a deviation from spherical symmetry, which is supported by some spectropolarimetric observations.

The following section will introduce examples for analytical and/or numerical calculations of polarized light and their results.

6.1 Modelling of linear polarization

Wood, Brown & Fox (1993) [85] analytically calculated polarimetric line profiles for **optically thin envelopes** in the case of pure electron scattering in non-relativistic bulk motion, with the assumption of a stellar point source. To model wavelength dependent polarization, one has to start with the knowledge of radiative transfer in the envelope.

They used a single scattering approximation (optically thin) and started with the time independent equation of radiative transfer for initially unpolarized light, which can be written as,

$$\hat{k} \cdot \nabla I_\nu = \rho^s j^s_\nu, \tag{6.1}$$

with $\hat{k}$ as the unit vector from the scattering element to the observer and I_ν the scattered Stokes vector $I_\nu = (I^S_\nu, I^Q_\nu, I^U_\nu, I^V_\nu)$. ρ^s is the mass density of scatterers and j^s_ν is the Stokes emission coefficient due to scattering:

$$j^s_\nu = \int_{\Omega_\star} \kappa^s_{\nu_\star} R_{\nu_\star}(\nu_\star, \hat{k}_\star; \nu, \hat{k}) I_{\nu_\star} d\Omega_\star. \tag{6.2}$$

$\kappa^s_{\nu_\star}$ is the scatterer opacity per unit mass, $I_{\nu_\star}$ is the incident Stokes vector at frequency $\nu_\star$, $\Omega_\star$ is the solid angle subtended at the scatterer by the source of radiation and $R_{\nu_\star}(\nu_\star, \hat{k}_\star; \nu, \hat{k})$ is the phase matrix which gives the probability of a photon of frequency $\nu_\star$, incident in solid angle $d\Omega_\star$, about direction $\hat{k}_\star$, being scattered with frequency ν into solid angle dΩ, about direction $\hat{k}$.

The phase matrix R_ν is wavelength independent for electron scattering and we can write:

$$R_{\nu_\star} = R$$

$$= \frac{3}{8\pi} \begin{pmatrix} \frac{1}{2}(1+\cos^2\chi) & \frac{1}{2}\sin^2\chi & 0 & 0 \\ \frac{1}{2}\sin^2\chi & \frac{1}{2}(1+\cos^2\chi) & 0 & 0 \\ 0 & 0 & \cos\chi & 0 \\ 0 & 0 & 0 & \cos\chi \end{pmatrix} \tag{6.3}$$

with χ the scattering angle: $\chi = \hat{k}_\star \cdot \hat{k}$.

Then 6.1 has the solution

$$I_\nu = \int_{l_1}^{l_2} \rho^S j^S_\nu dl. \tag{6.4}$$

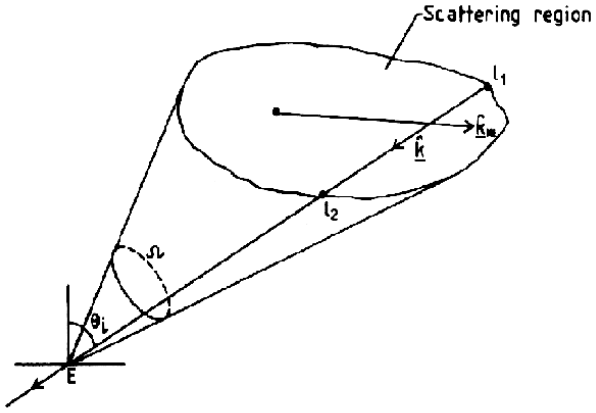

Figure 6.1: Intensity scattered from direction $\hat{k}_\star$ into the observer direction $\hat{k}$. The specific intensity at earth, E, is obtained by integrating $\rho^s j_\nu^s$ through the scattering region from l_1 to l_2. Θ_i is the angle beween the observer direction and the normal to the surface at E, and Ω is the solid angle subtended by the entire scattering region at the earth (Wood, Brown & Fox, 1993).

Figure 6.1 shows a sketch for the scattering event.

The observed Stokes vector is the line integral of $\rho^S j_\nu^S$ along the line-of-sight, $\hat{k}$, through the scattering region, under the assumption of no additional scattering or absorption event.

The energy passing through area $dA\cos\Theta_i$ is given by

$$F_\nu = \int_\Omega I_\nu \cos\Theta_i d\Omega, \tag{6.5}$$

where Θ_i is the angle between the incident radiation and the normal to the surface dA. The flux vector becomes $F_\nu = (F_\nu^S, F_\nu^Q, F_\nu^U, F_\nu^V)$ and the flux is an integral over the scattering region length and the solid angle:

$$F_\nu = \int_\Omega \int_{l_1}^{l_2} \rho^S j_\nu^S \cos\Theta_i dl\, d\Omega. \tag{6.6}$$

The scattering range is much smaller than the observer's distance D and if the area dA is perpendicular to the incident radiation then $\cos\Theta_i = 1$. With $l^2\, dl\, d\Omega = dV_\star$ we get:

$$F_\nu = \frac{1}{D^2} \int_{V_\star} \rho^S j_\nu^S dV_\star. \tag{6.7}$$

After a transformation for the entire scattering region and the correction for a moving scatterer due to stellar wind motion they found the following expressions for the normalized Stokes parameters:

$$Q_\nu = \frac{F_\nu^Q}{F_\nu^D + F_\nu^S}, \quad U_\nu = \frac{F_\nu^U}{F_\nu^D + F_\nu^S}. \tag{6.8}$$

F_ν^D is the direct flux and F_ν^S is the scattered flux. For a single scattering event $F_\nu^S \ll F_\nu^D$ and one can write:

$$Q_\nu \approx \frac{F_\nu^Q}{F_\nu^D}, \quad U_\nu = \frac{F_\nu^U}{F_\nu^D}, \tag{6.9}$$

where, in the point source approximation,

$$F_\nu^D = \int_\Omega I_\nu d\Omega \approx \frac{\pi R^2}{D^2} I_\nu. \tag{6.10}$$

R is the radius of the source ($R \ll r$). The Doppler correction for the stellar wind is

$$\nu = \left(\frac{1-\beta\cdot\hat{k}_\star}{1-\beta\cdot\hat{k}}\right)\nu_\star. \tag{6.11}$$

They applied their method to Be stars, with a stellar point source approximation and a scattering, optically-thin, equatorial disk with inclination i to the observer. They investigated a rotating and an expanding disk with the velocity expressions

$$V_\phi(r) = V_0 \left(\frac{R}{r}\right)^{1/2} \tag{6.12}$$

and

$$V_r(r) = V_1 + V_\infty \left(1 - \frac{R}{r}\right)^{1/2}. \tag{6.13}$$

For a pure rotational disk the density distribution is

$$\sum(r) = \sum_0 \left(\frac{R}{r}\right)^2, \tag{6.14}$$

with $\sum_0$ as the density at the star-disk boundary. Their input line profile is a gaussian superposed on a continuum at wavelength λ_0 with the intensity

$$I_{\nu_\star} = I_0 \left[1 + \alpha \exp - \left(\frac{\lambda_\star - \lambda_0}{\lambda_b}\right)^2\right]. \tag{6.15}$$

$\lambda\star$ is the wavelength emitted by the star , λ_0 is the rest wavelength and λ_b is the width of the stellar line. After a Doppler correction between $\lambda\star$ and the observed wavelength λ with respect to the inclination of the star, they get the Stokes parameters Q and U as

$$\begin{aligned}\left\{\begin{array}{c} Q_\nu \\ U_\nu \end{array}\right\} &= \frac{P_0}{\left[1 + \alpha \exp - \left(\frac{\lambda_\star - \lambda_0}{\lambda_b}\right)^2\right]} \\ &\times \int_{A_\star} \left(1 + \alpha e^{-\{A(r,\phi,\lambda)\}^2}\right) \\ &\times f(r) \left\{\begin{array}{l} \sin^2 i - (1+\cos^2 i)\cos 2\phi \\ 2\cos i \sin 2\phi \end{array}\right\} \frac{dA_\star}{r^2}\end{aligned} \tag{6.16}$$

with the density distribution

$$P_0 = \frac{3\sigma_T \sum_0}{32\,\pi} \tag{6.17}$$

The area $A_\star$ is the area of the disk minus the area occulted by the star and the integral operator is

$$\int_{A_\star} = \int_1^{\alpha_D} \int_0^{2\pi} - \int_1^{\delta} \int_{\pi/2+\phi(x)}^{3\pi/2-\phi(x)}, \qquad (6.18)$$

with $\delta = \sec i$ for $\alpha_D \sec i$ and $\delta = \alpha_D$ for $\alpha_D < \sec i$, with the radius of the disk α_D in stellar radii.

With the input profile of photospheric origin, given in Eq. 6.15 with $\alpha = 2$, $\lambda_0 = 6562\,\text{Å}$ and $\lambda_b = 4\,\text{Å}$ (Fig. 6.2), they calculated output profiles Fig. 6.3, 6.5 and 6.7 for a pure Keplerian rotating disk, a pure expanding disk, and an expanding and rotating disk, respectively. Each plot is for a point source with and without occultation. Also their isowavelength-shift contours (Fig. 6.4, 6.6 and 6.8) are given.The stellar parameters are $\alpha_D = 10$, $V_0 = 360\text{km/s}$ and $V_\infty = 90\text{km/s}$.

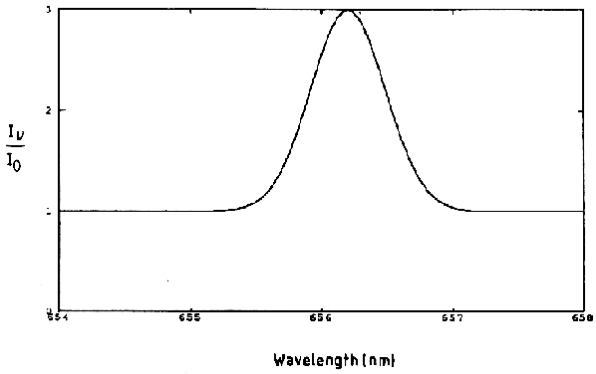

Figure 6.2: Initial photospheric broadened line profile at 6562 Å (Hα) normalized by continuum specific intensity (Wood, Brown & Fox, 1993).

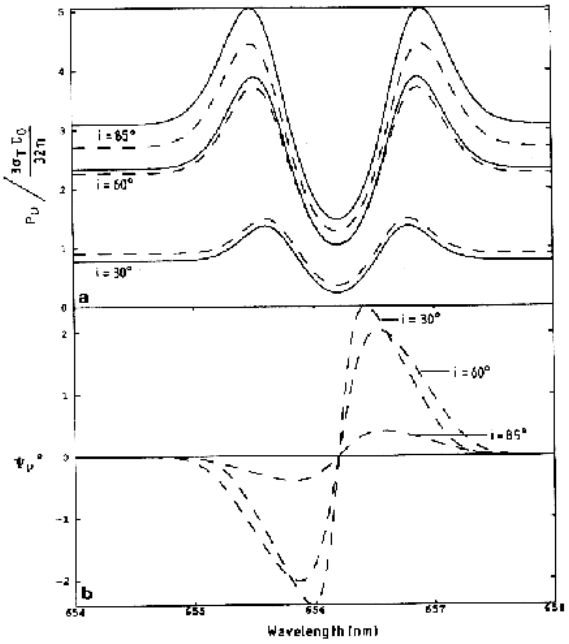

Figure 6.3: (a) Linear polarization and (b) position angle, against wavelength for a pure Keplerian rotating disk. The solid curve is for a point source without and the dashed curve is for a point source with occultation effects included. The pairs of curves are for inclinations 30°, 60°, and 85°. (Wood, Brown & Fox, 1993).

For **optically thick envelopes**, like Wolf-Rayet winds, including electron-scattering and thermal opacities, a qualitative model was developed by Schulte-Ladbeck et al. (1992a [65]) in their paper about HD 191765, which is illustrated in Fig. 6.9.

The basis of this model is the supression of polarization due to multiple scattering. This means that almost all polarization is introduced by the *last scattering*, which occurs above the $\tau_{es} = 1$ radius. They state that in WR winds the radius at which the average photon of a given wavelength is created from thermal emission (the thermalization depth) is different from the last scattering radius. In the case of electron scattering as the major contributor to the opacity, the stellar radius may be defined as the distance where $\tau_{es} \approx 1$. For wavelengths where bound-free and free-free opacities dominate electron scattering, a different stellar radius is defined by $\tau_{th} = 1$. The thermal opacities increase with wavelength and so the stellar radius is larger in the IR than in the UV.

A purely numerical model for optically thick lines to interpret polarization observations of stars showing extensive winds such as LBVs and Wolf-Rayet stars has been developed recently by Hillier (1996 [28]). Allowing for (a) *stratification effects*, (b) *multiple scattering*, (c) *line formation processes* which affect the line polarization due to different opacities and (d) *frequency redistribution* due to bulk and thermal motions of the scattering electrons, Hillier developed a transfer code and an independent Monte-Carlo code which can test the numerical code. Because circular polarization obeys a different and separate transfer equation from that of the other three Stokes parameters and because electron scattering does not create circular polarized light, he did not discuss this case.

Starting with the source function for pure electron scattering and a redistribution function, which describes the scattering of light of one particular state (direction, polarization and frequency) into another state, he uses wavelength dependent comoving frame transfer functions. The boundary conditions are the following:

1. For rays striking the outer boundary the incident radiation field is zero.
2. For rays striking an optically thick inner boundary (such as a stellar surface), the diffusion approximation is adopted, or the outward intensity is specified.

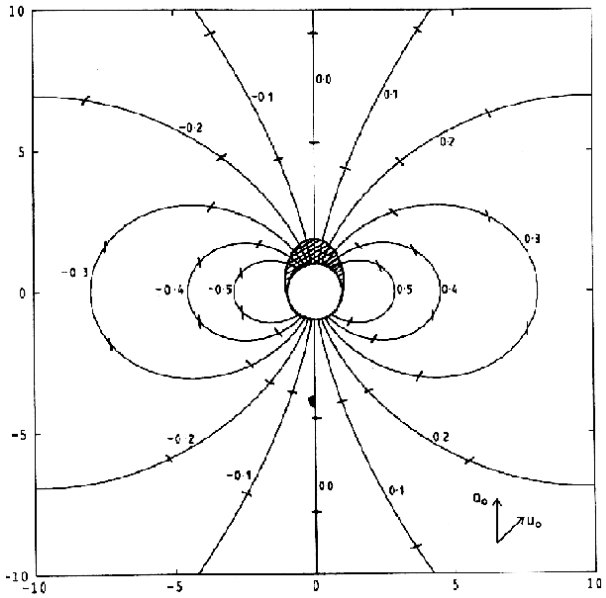

Figure 6.4: Isowavelength-shift contours, $\frac{\lambda-\lambda_*}{\lambda_*} \times 10^{-3}$ = constant, on a Keplerian disk viewed by an observer inclined at 60° to the rotation (z) axis and positioned at infinity in the x-z plane. The hatched region is the area of the disk occulted by the star. The axes are labelled in units of stellar radii. The short bars are the projections upon the sky of the direction of vibration of the local polarization vector for different disk regions. The positive Stokes Q and U directions chosen for the entire system are also shown, (Q_0, U_0) (Wood, Brown & Fox, 1993).

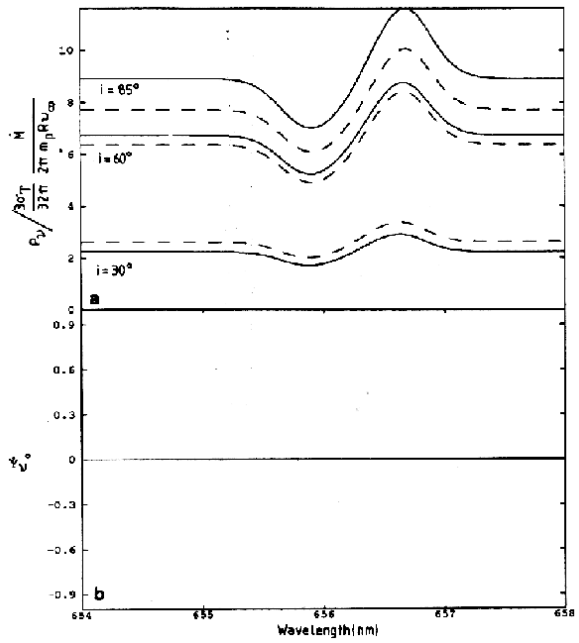

Figure 6.5: (a) Linear polarization and (b) position angle against wavelength for the disk velocity being purely expansional (Wood, Brown & Fox, 1993).

The solution technique for the polarized transfer function at every point of the atmosphere proceeds as follows:

1. Solve the continuum polarized transfer equation for the continuum source function.
2. At the chosen grid point , solve the polarized transfer equation for the continuum intensity along a single ray.
3. Solve for the radiation field at all frequencies integrating from the blue to the red.
4. Repeat procedures 2 and 3 for all rays passing through the grid point.
5. Perform the frequency redistribution in order to compute the "frequency" averaged moments necessary for the computation of the electron scattering source function.
6. Repeat steps 2–5 for all spatial grid locations.
7. Perform an Ng acceleration (Ng 1974 [50], Auer 1987 [1]) if reqired.
8. Repeat steps 2–7 until convergence of the electron scattering source function has been obtained.
9. Using a separate code, compute the polarized line profiles as a function of viewing inclination.

With this procedure, Hillier calculated polarization line profiles for the cases of (a) pure electron scattering, (b) electron scattering with line opacity, (c) Wolf-Rayet models, (d) the He II 5411 Å line, (e) the He II 1640 Å line, (f) inclination effects and (g) a "thick disk" with a half opening angle of 7° applied to WR stars. Stellar rotation was neglected for this model which can lead to non-zero flux for Stokes U and to a variation in position angle across the line.

One of his results is given in Fig. 6.10 for the He II 5411 Å line of the Wolf-Rayet model.

Recent model calculations for multiple Thomson scattering processes in optically thick atmospheres have been published by Wood et al. (1996 [86]). It was often assumed that multiple scattering will reduce the polarization. But as a very interesting result, they find that multiple scattering in the envelope *increases* the polarization above the "single scattering plus attenuation" approximation, introduced in single scattering models.

The calculation, based on a Monte-Carlo simulation, was applied to unresolved, axisymmetric geometries in the plane-parallel atmosphere approximation. The calculations were done for the following geometries:

- For geometrically thin disks: A finite source plus

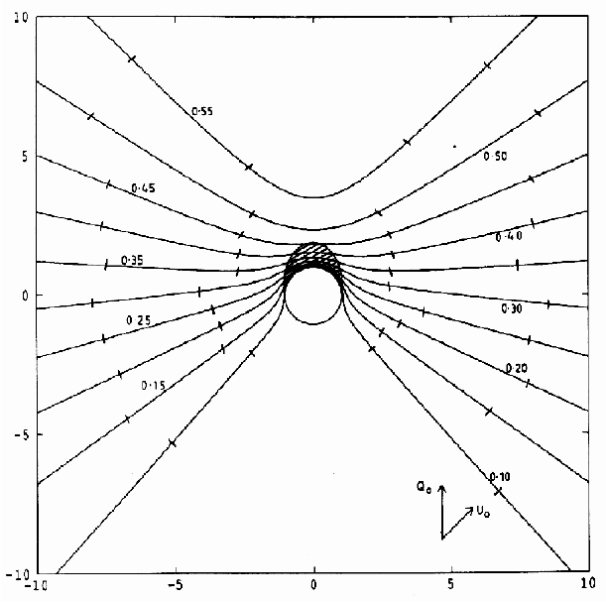

Figure 6.6: Isowavelength-shift contours for the disk velocity being purely expansional (Wood, Brown & Fox, 1993).

a geometrically thin disk.

- For geometrically thick disks: A finite source plus an ellipsoidal envelope.
- For polar jets and plumes: A narrow jet.
- For polar jets and plumes: A wide jet.

Wood et al. conclude that one has to be very careful with constraints on circumstellar geometries from polarization observations, if single scattering or point-source approximations are used. Multiple scattering can have a dramatic effect on the predicted polarization levels, even reversing the sign (i.e., causing a 90° flip in the position angle). In addition, they found that point-source approximations yield lower polarization levels than finite-source approximations, in the case of multiple scattering in optically thick environments. As an example, one can easily see from Tables 6.1 and 6.2 the difference between point and finite sources. The tables give the numbers in percent of unscattered and scattered photons and the average number of scatterings for both a finite source and a point source.

The largest deviations are found for large opacities at the equator as well as at the pole.

Table 6.1: Percentage of scattered and unscattered photons and the mean number of scatterings for a point source

τ_{eq}	τ_{pole}	unscattered photons in %	scattered photons in %	average number of scatterings
1.0	0.01	94.52	5.48	1.15
2.0	0.02	90.38	9.62	1.30
3.0	0.03	87.08	12.92	1.43
4.0	0.04	84.38	15.62	1.57
5.0	0.05	82.12	17.88	1.70
6.0	0.06	80.18	19.82	1.82
7.0	0.07	78.47	21.53	1.94
8.0	0.08	76.96	23.04	2.07
9.0	0.09	75.71	24.39	2.19
10.0	0.10	74.36	25.64	2.31

Table 6.2: Percentage of scattered and unscattered photons and the mean number of scatterings for a finite source

τ_{eq}	τ_{pole}	unscattered photons in %	scattered photons in %	average number of scatterings
1.0	0.01	96.09	3.91	1.15
2.0	0.02	93.78	6.22	1.30
3.0	0.03	92.23	7.762	1.44
4.0	0.04	91.05	8.95	1.59
5.0	0.05	90.06	9.94	1.72
6.0	0.06	89.20	10.80	1.85
7.0	0.07	88.39	11.61	1.98
8.0	0.08	87.62	12.38	2.09
9.0	0.09	86.88	13.11	2.21
10.0	0.10	86.18	13.82	2.32

6.2 Modelling of circular polarization

The modelling of circularly polarized light concerns internal magnetic fields. We have to find a connection between the field strength B and Stokes V. An analytical approach has been done by Landstreet (1982 [35])

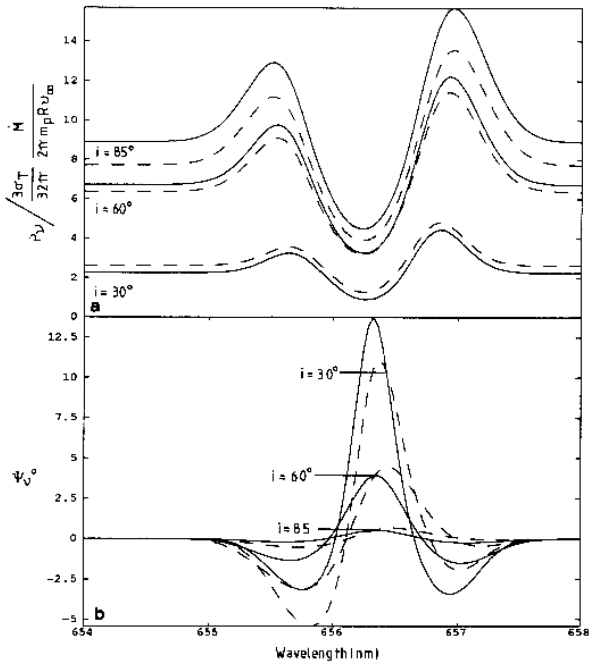

Figure 6.7: (a) Linear polarization and (b) position angle against wavelength for a rotating and expanding disk (Wood, Brown & Fox, 1993).

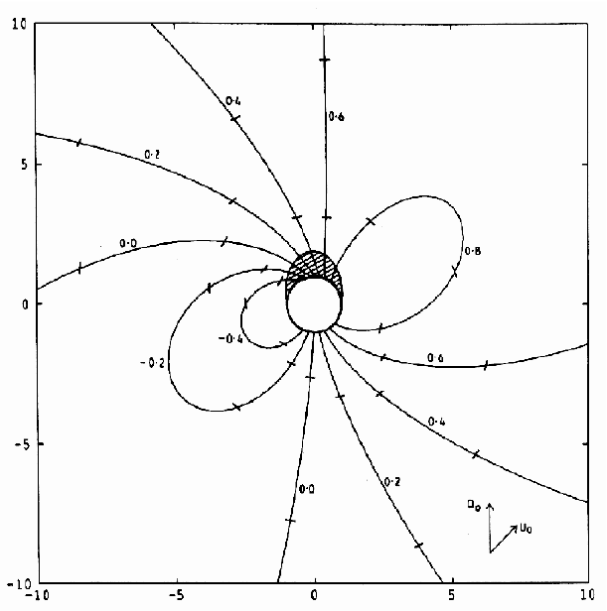

Figure 6.8: Isowavelength-shift contours for a rotating and expanding disk (Wood, Brown & Fox, 1993).

in the context of a search for magnetic fields in upper-main sequence stars. A strong argument for the existence of fields in upper-main sequence stars comes from the tremendous fields of pulsars ($B \sim 10^{12} - 10^{13}$ G) and white dwarfs ($B \sim 10^{7}$ G). If stars with masses within the range 5 to 8 $M_{\odot}$ collapse to pulsars with such fields, their initial field must have values of the order $10^{2} - 10^{3}$ G.

To estimate the strength of a magnetic field from observations of circularly polarized light, we have to start with the expression

$$I(\lambda, \Theta) = B_0[1 + \beta \cos\Theta(1+\eta)^{-1}] \qquad (6.19)$$

and

$$\begin{aligned} V(\lambda, \Theta) &= B_0 \beta \cos\Theta \Delta\lambda_B \cos\psi \eta'(1+\eta)^{-2} \\ &= \Delta\lambda_B \cos\psi dI(\lambda,\Theta)/d\lambda \end{aligned} \qquad (6.20)$$

where B_0 is a constant, $\Delta\lambda_B$ is the Zeeman separation, ψ is the angle between the magnetic field vector and the line-of-sight, Θ is the angle between the local surface normal and the line-of-sight, η is the ratio of line to continuum opacity, and β is a constant. In the case of spatially unresolved stellar light, we have to integrate these equations over the visible hemisphere. But then, the polarization profiles from various parts of the disk will be Doppler shifted due to stellar rotation. Also ψ and $\Delta\lambda_B$ vary over the stellar disk. Landstreet's approximation is to ignore the Doppler shift of the polarization profiles with the assumption of a small $\Delta\lambda_i$ compared to the velocity broadening of the line. Following this approximation, integration gives

$$\bar{I} = \frac{1}{\pi}\int_0^{2\pi} d\Phi \int_0^{\pi/2} \cos\Theta \sin\Theta I(\lambda,\Theta) d\Theta \qquad (6.21)$$

and

$$\begin{aligned} \bar{V} &= \frac{1}{\pi}\int_0^{2\pi} d\Phi \int_0^{\pi/2} \cos\Theta \sin\Theta \Delta\lambda_B \cos\psi(\Theta,\phi) \\ &\quad \times [dI(\lambda,\Theta)/d\lambda] d\Theta \end{aligned} \qquad (6.22)$$

A line-strength weighted effective field, which is more strongly weighted toward the center of the stellar disk than the usual limb-darkening weighted effective field, implies that a longitudinal field measured by the Zeeman effect will sample the field more strongly at the disk center, where the line is strong. Introducing the instrumental broadening function $F(\lambda - \lambda')$ Landstreet found

$$d\bar{I}_0(\lambda)/d\lambda = \int F(\lambda - \lambda')[d\bar{I}(\lambda')/d\lambda'] d\lambda'. \qquad (6.23)$$

and

$$\bar{V}_0(\lambda)/\bar{I}_0 = \Delta\lambda_l (d\bar{I}_0/d\lambda)/\bar{I}_0 \qquad (6.24)$$

The last equation has been generally used to interpret photoelectric Zeeman polarization measurements, and Landstreet found that it is (with some restrictions)

approximately valid even in the presence of a nonuniform magnetic field and instrumental line broadening.

A numerical simulation of Zeeman-Doppler imaging to detect magnetically active late-type stars is given by Donati et al. (1989 [18]). The general hypothesis was (a) the star is assumed to be spherical and rotates as a rigid body; (b) the local profile is assumed to be identical all over the stellar photosphere; and (c) the observed magnetically sensitive line is a triplet.

For instance, they calculated that in a star with $v \sin i = 32\,\mathrm{km/s}$, a line at 6000 Å with g=2 can be used to detect a 1000 G single magnetic spot covering 10% of the visible surface, provided S/N ≥ 350 per 0.08 Å pixel.

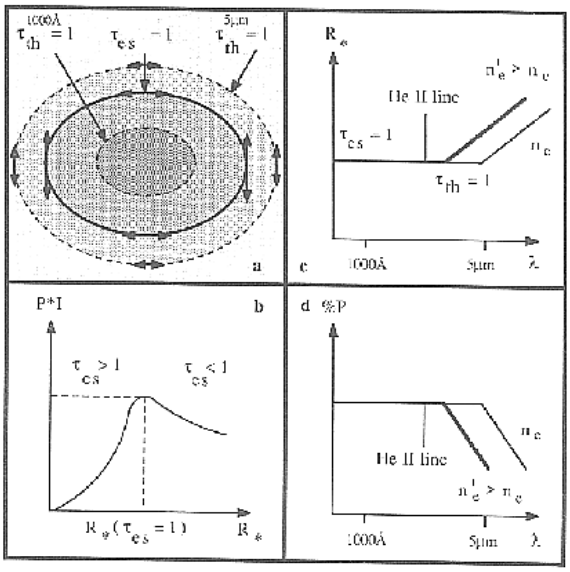

Figure 6.9: Optically thick wind model with an ellipsoidal density distribution and an observer located in the equatorial plane. (a) The radius of creation, $\tau_{th}(\nu) = 1$, at a given frequency is different from the radius of last scattering $\tau_{es} = 1$. For all photons with $\tau_{th}(\nu) < \tau_{es} \approx 1$(e.g., at 1000 Å), the radius of the star is the same, namely the radius of last scattering; at long wavelengths (e.g., 5μm) the photons are created outside the $\tau_{es} = 1$ layer. (b) Inside the $\tau_{es} = 1$ radius, multiple scattering destroys the polarization. The maximum polarization is reached at $\tau_{es} \approx 1$. The observer sees a polarized star. (c) The radius of the star is a function of wavelength. Emission lines (e.g., of HeII) are always formed at larger radii than the continuum. (d) The larger the formation radius, the smaller the electron-scattering optical depth from the radius out to infinity and the smaller is the polarization (continuum and lines). Note the prediction of a turnover in the polarization spectrum depending on wind density (n_e or n'_e) (Schulte-Ladbeck et al., 1992a).

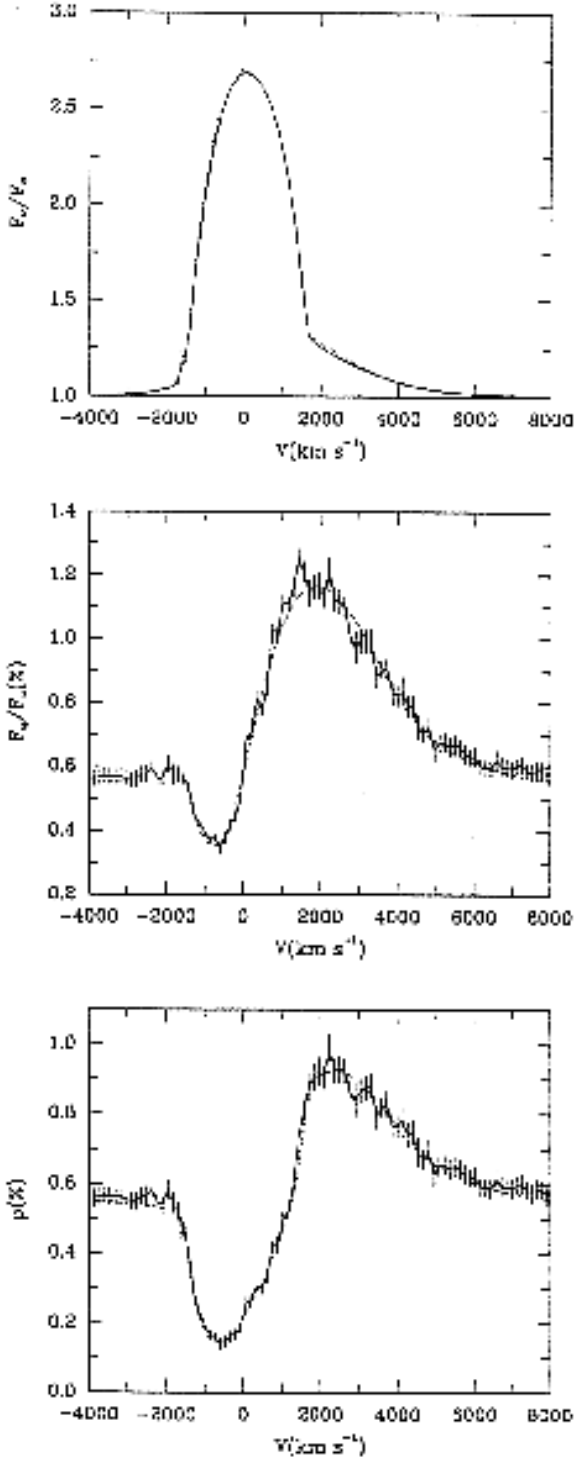

Figure 6.10: The normalized He II 5411 Å line profile F_ν/F_c, the polarized flux F_q/F_c in percent, and the percentage polarization $P = F_q/F\nu$. Note the enhanced polarization in the red line wing, and the strong depolarization across the line. The solid curve illustrates the results obtained with the Monte-Carlo code, with statistical error bars of $\pm 1\sigma$ indicated (Hillier, 1996).

Chapter 7

Practical considerations

7.1 The Mueller calculus

The Mueller calculus (Mueller 1943) is a matrix-algebraic method of specifying a beam of light and the optical devices encountered by the beam, and computing the outcome. If light passes a number of polarizers and/or retarders, conventional algebraic methods become extremely complicated; the arithmetic required is voluminous and the procedure is different for each different problem. The Mueller calculus on the other hand uses the fact that it is possible to

(a) condense all the necessary parameters for describing a light beam, polarizer, retarder or scatterer *into a single package* at a time, and

(b) to provide a set of rules where the result of interposing any number of optical elements can be *determined by multiplying the used packages in a standard manner.*

Thus the outcome of any experiment can be determined by a fixed procedure: selecting the appropriate packages from a table and simply multiplying them together.

The standard light beam description is simply a four-parameter Stokes vector (I, Q, U, V) and optical devices (polarizer, retarder, etc.) are described by the so called *Mueller matrix*, a 4×4 transformation matrix. For ideal devices most of the elements are zero, which makes the calculation very easy. The individual matrix deals not only with the composition of the device but also with its *orientation.* For instance, a linear polarizer with a horizontal transmission axis has a different Mueller matrix than a linear polarizer which is turned by some degrees.

The Mueller calculus follows the rules for matrix-algebra and the vector representing the incident beam must be written "at the right".

For example, the calculation of the Stokes paramaters of a beam which passed a retarder *followed* by a polarizer is described in matrix-algebra by:

$$\begin{pmatrix} I' \\ Q' \\ U' \\ V' \end{pmatrix} = \begin{pmatrix} p_{11} & p_{12} & p_{13} & p_{14} \\ p_{21} & p_{22} & p_{23} & p_{24} \\ p_{31} & p_{32} & p_{33} & p_{34} \\ p_{41} & p_{42} & p_{43} & p_{44} \end{pmatrix}_{pol} \times \begin{pmatrix} r_{11} & r_{12} & r_{13} & r_{14} \\ r_{21} & r_{22} & r_{23} & r_{24} \\ r_{31} & r_{32} & r_{33} & r_{34} \\ r_{41} & r_{42} & r_{43} & r_{44} \end{pmatrix}_{ret} \times \begin{pmatrix} I \\ Q \\ U \\ V \end{pmatrix} \tag{7.1}$$

7.2 The retarder matrix

A general description of Mueller matrices for retarders and polarizers was given by Serkowski (1962) [71]: By cutting a calcite or quartz crystal parallel to its optical axis one can produce an optical element which introduces a phase-shift between the two components of the E vector vibrating in the planes of the l and r direction. The introduced phase-shifts

$$\tau = \epsilon_l - \epsilon_r \tag{7.2}$$

are 180° and 90° for a $\lambda/2$ and a $\lambda/4$ plate, respectively.

If the redardation plate is rotated counterclockwise by the angle ψ, **the retardation matrix** acquires the form

$$R = \begin{pmatrix} 1 & 0 & 0 & 0 \\ 0 & \cos^2 2\psi + \sin^2 2\psi \cos\tau & (1-\cos\tau)\cos 2\psi \sin 2\psi & -\sin 2\psi \sin\tau \\ 0 & (1-\cos\tau)\cos 2\psi \sin 2\psi & \sin^2 2\psi + \cos^2 2\psi \cos\tau & \cos 2\psi \sin\tau \\ 0 & \sin 2\psi \sin\tau & -\cos 2\psi \sin\tau & \cos\tau \end{pmatrix} \tag{7.3}$$

In this context one can easily calculate the Mueller matrices for an ideal plate of isotropic, nonabsorbing glass (M_1); for an ideal plate of isotropic, absorbing glass whose transmittance is k (M_2); and for a totally absorbing plate (M_3) :

$$M_1 = \begin{pmatrix} 1 & 0 & 0 & 0 \\ 0 & 1 & 0 & 0 \\ 0 & 0 & 1 & 0 \\ 0 & 0 & 0 & 1 \end{pmatrix}$$

(7.4)

$$M_2 = \begin{pmatrix} k & k & k & k \\ k & k & k & k \\ k & k & k & k \\ k & k & k & k \end{pmatrix}$$

(7.5)

$$M_3 = \begin{pmatrix} 0 & 0 & 0 & 0 \\ 0 & 0 & 0 & 0 \\ 0 & 0 & 0 & 0 \\ 0 & 0 & 0 & 0 \end{pmatrix}$$

(7.6)

7.3 The polarizer matrix

An ideal polarizer, which transmits only the vibrations in the plane making an angle φ, has the following form:

$$P = \frac{1}{2} \begin{pmatrix} 1 & \cos 2\varphi & \sin 2\varphi & 0 \\ \cos 2\varphi & \cos^2 2\varphi & \cos 2\varphi \sin 2\varphi & 0 \\ \sin 2\varphi & \cos 2\varphi \sin 2\varphi & \sin^2 2\varphi & 0 \\ 0 & 0 & 0 & 1 \end{pmatrix}$$

(7.7)

In the case of an element which splits the two mutually perpendicular beams, that are phase shifted by the angle τ after passing the retarder (e.g., a Nicol prism), the polarizer matrix acquires a simple form. For the ordinary Beam, indicated by $\parallel$, we have $\varphi = 0°$ and for the extraordinary beam, indicated by $\perp$, we have $\varphi = 90°$. Then the Mueller matrices become:

$$M_{\parallel} = \frac{1}{2} \begin{pmatrix} 1 & 1 & 0 & 0 \\ 1 & 1 & 0 & 0 \\ 0 & 0 & 0 & 0 \\ 0 & 0 & 0 & 0 \end{pmatrix}$$

(7.8)

$$M_{\perp} = \frac{1}{2} \begin{pmatrix} 1 & -1 & 0 & 0 \\ -1 & 1 & 0 & 0 \\ 0 & 0 & 0 & 0 \\ 0 & 0 & 0 & 0 \end{pmatrix}$$

(7.9)

A number of different beam-splitting analyzers is shown in Fig. 7.1.

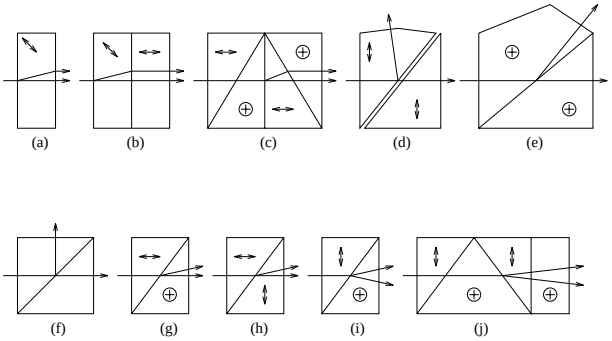

Figure 7.1: Beam–splitting analyzers: (a) plane-parallel calcite plate; (b) double calcite plate; (c) double Rochon prism; (d) Glan-Foucault prism (modified by Archard and Taylor); (e) Glan-Thompson (Foster) prism; (f) thin-film polarizing beam-splitter; (g) Rochon prism; (h) Senarmont prism; (i) Wollaston prism; (j) three-wedge Wollaston prism. The directions of light beams and the directions of crystallic optical axes are indicated by arrows; the circled crosses denote the optical axis perpendicular to the plane of the drawing (Serkowski, 1974).

7.4 The William-Wehlau-Spectropolarimeter

The William-Wehlau-Spectropolarimeter † (we also call it "The Stokes Meter") is a combination of a retarder consisting of two $\lambda/4$ plates and a Wollaston Prism as polarizer, leading into a CCD spectrograph. The instrument was developed and built at the University of London/Ontario in collaboration with the Universities of Brandon/Manitoba and Montréal/Québec. Figure 7.2 shows the design of the polarimeter unit and Figure 7.3 the open polarizer in the laboratory.

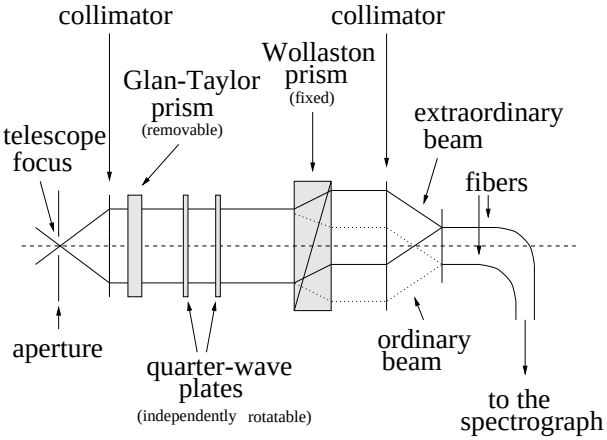

Figure 7.2: Simple sketch of the Stokes-Meter.

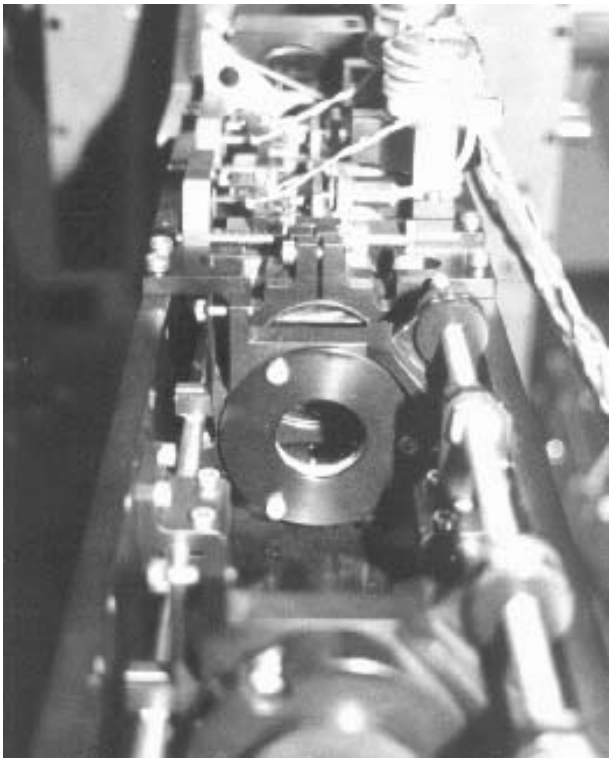

Figure 7.3: View onto the Stokes-Meter optics.

At the heart of the instrument are the two $\lambda/4$ plates which act as retarders and introduce a 90° shift between the mutually orthogonal components of the partially polarized beam. Figure 7.4 shows one of these plates in the center of a worm removed from the Stokes Meter, while Figure 7.5 shows both plates installed in the instrument.

The plates are rotatable via stepping motors to different angles ψ (see chapter 7.2). They are controled by a software written in C++ by N. Piskunov and implemented on a personal computer. After passing the two plates, the retarded beam crosses the polarizer which is here a Wollaston Prism, were the beam is split into an ordinary beam (which follows the refraction law) and an extraordinary beam (which does not).

The two beams then reach the two fibers which feed the spectrograph slit. The light path in the spectrograph is identical with the standard way to obtain a spectrum, except that we now have two spectra: that of the ordinary beam, $I_o(\lambda)$, and that of the extraordinary beam $I_e(\lambda)$, aligned parallel on the detector. From these wavelength dependent spectra, $I_\parallel$ (parallel) and $I_\perp$ (perpendicular), we can, by combining data for various combinations of orientations of the $\lambda/4$ retarders, obtain the four Stokes parameters $I_{total}(\lambda), Q(\lambda), U(\lambda)$ and $V(\lambda)$ via the Mueller calculus.

To test for cross talk between the beams and for possible non-linearity in the $\lambda/4$ plates, a removable Glan-Taylor prism which produces nearly 100% linearly polarized light at all optical wavelengths is installed in front of the retarders. Fast axes of $\lambda/4$ plates must first be aligned with the axis of the Wollaston prism. This can be automatically done by the computer program.

Following the Mueller calculus and the rules for matrix algebra, we can calculate the four Stokes parameters for this arrangement with $\tau = 90°$ for both $\lambda/4$ plates. With $\mathbf{A}$ and and $\mathbf{A}'$ as the Stokes vectors before and after passing the retarder plates $\mathbf{R}_1$ and $\mathbf{R}_2$, and the polarizer $\mathbf{P}$, we use the *Ansatz* (cf. 8.1):

$$\mathbf{A}' = \mathbf{P} \times \mathbf{R_2} \times \mathbf{R_1} \times \mathbf{A} \qquad (7.10)$$

Following this expression for different angular positions of the optical elements, we get a number of resulting equations for the final, observed Stokes parameter I that contains all the information we need on I, Q, U and V of the original beam (A). If we indicate the intensity with the angular values of retarder one, retarder two and the position of the polarizer ($\parallel$ or $\perp$), in this order; F as the time-dependent variation (e.g., seeing,

†After the principal investigator William Wehlau, Professor at the University of Western Ontario (UWO) (1961 - 1995), deceased.

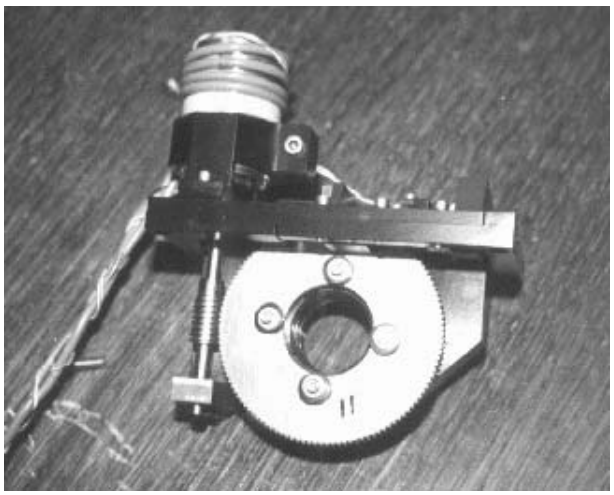

Figure 7.4: One $\lambda/4$ (retarder) plate removed from the Stokes-Meter.

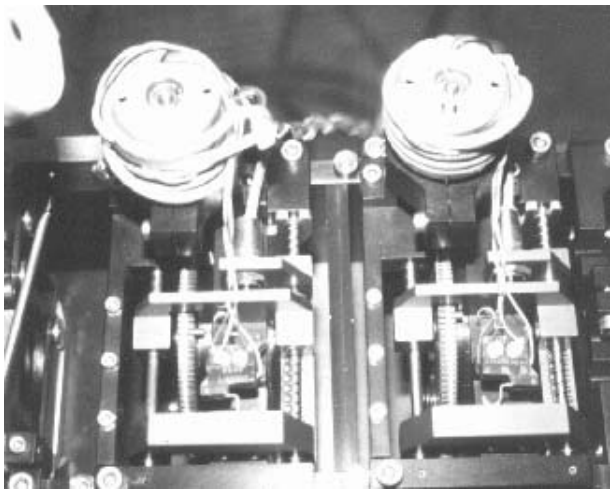

Figure 7.5: The $\lambda/4$ plates and the stepping motors placed in the polarizer unit.

transparency); and G the angular position dependent gain factor; we have, for instance:

$$I'_{0,0,\|} = 1/2(I+Q)F_{0,0}G_{\|} \quad (7.11)$$
$$I'_{0,0,\perp} = 1/2(I-Q)F_{0,0}G_{\perp} \quad (7.12)$$
$$I'_{45,45,\|} = 1/2(I-Q)F_{45,45}G_{\|} \quad (7.13)$$
$$I'_{45,45,\perp} = 1/2(I+Q)F_{45,45}G_{\perp} \quad (7.14)$$
$$I'_{0,45,\|} = 1/2(I+U)F_{0,45}G_{\|} \quad (7.15)$$
$$I'_{0,45,\perp} = 1/2(I-U)F_{0,45}G_{\perp} \quad (7.16)$$
$$I'_{0,-45,\|} = 1/2(I-U)F_{0,-45}G_{\|} \quad (7.17)$$
$$I'_{0,-45,\perp} = 1/2(I+U)F_{0,-45}G_{\perp} \quad (7.18)$$
$$I'_{-45,0,\|} = 1/2(I+V)F_{-45,0}G_{\|} \quad (7.19)$$
$$I'_{-45,0,\perp} = 1/2(I-V)F_{-45,0}G_{\perp} \quad (7.20)$$
$$I'_{45,0,\|} = 1/2(I-V)F_{45,0}G_{\|} \quad (7.21)$$
$$I'_{45,0,\perp} = 1/2(I+V)F_{45,0}G_{\perp} \quad (7.22)$$

With these equations we can easily get the intensity-normalized Stokes parameters Q, U and V:

$$\frac{Q}{I} = \frac{R_Q - 1}{R_Q + 1} \quad (7.23)$$
$$\frac{U}{I} = \frac{R_U - 1}{R_U + 1} \quad (7.24)$$
$$\frac{V}{I} = \frac{R_V - 1}{R_V + 1} \quad (7.25)$$

with

$$R_Q = \sqrt{\frac{I'_{0,0,\|} \cdot I'_{45,45,\perp}}{I'_{0,0,\perp} \cdot I'_{45,45,\|}}} \quad (7.26)$$
$$R_U = \sqrt{\frac{I'_{0,45,\|} \cdot I'_{0,-45,\perp}}{I'_{0,45,\perp} \cdot I'_{0,-45,\|}}} \quad (7.27)$$
$$R_V = \sqrt{\frac{I'_{-45,0,\|} \cdot I'_{45,0,\perp}}{I'_{-45,0,\perp} \cdot I'_{45,0,\|}}} \quad (7.28)$$

Note that these double ratios are impervious of both time dependent variations and spatially dependent gain factors, as long as the two beams are obtained simultaniously on the same part of the detector each time. They should therefore be purely photon-noise limited. The intensity I within a constant is easy to get from a simple addition of corresponding pairs of equations, after appropriate determination of the gain factors by flat-fielding. Also note that any of the angles ψ of the $\lambda/4$ plates can be replaced by $\psi \pm 180°$ with identical results, providing the surfaces of the plates are not inclined to the optical axis (Serkowski, 1974 [70]). If the $\lambda/4$ plates are not exactly $\tau = 90°$, the above equations must be modified; this can be done for small deviation from $\tau = 90°$.

Chapter 8

Conclusions and final remarks

Because of the different mechanisms of producing linear and circular polarization, we have the tools to detect two different effects. The detection of linear polarization leads to general information on the material geometry in the circumstellar environment, caused, e.g., by turbulence of the wind and deviation from spherical symmetry, or ionization stratification. The detection of circular polarization tells us about magnetic fields and their geometry. Such fields have been detected so far only in peculiar B and A stars.

These tools support the picture of a turbulent, non-isotropic wind, which shows deviation from spherical symmetry and ionization stratification.

The advantage of spectropolarimetry lies mainly in the detection of different wavelength ranges, and that means in the context of hot stars, the detection of different ionization stages in different distances from the stellar surface. Thus, it should be possible to get a three-dimensional image of the target star. That is not otherwise possible. Applied to Be stars, detection of polarization of the disk lines leads to improved understanding of the connection between photospheric processes and the disk itself; how can we understand the observed oscillation of the disk, which comes and goes in timescales of years in the frame of a stable wind-compressed disk? For Wolf-Rayet stars, with their hidden surface, what is the connection between the surface and the wind? Is it possible to get a deeper view into the optically thick envelope? How far can we detect and describe the fields of magnetic stars? Is it possible to detect microfield structures near the surface? Can we detect magnetic fields in Wolf-Rayet stars and if yes, what role do they play in the frame of stellar winds?

The theoretical background of both linear and circular polarization is still not well developed. Numerical calculations have yielded significant progress in understanding the geometry and structure of magnetic fields in hot stars. For instance, in the qualitative model of Schulte-Ladbeck et al., a reduction of polarized light was assumed if multiple scattering plays a role, whereas the numerical calculations of Wood et al. show that this is not the case.

There are still very few observations in spectropolarimetric mode and many questions which have to be answered, but the application is clear. Hot stars are worthy targets for polarization diagnostics.

A technique which uses new ways to increase our understanding of nature can have a tremendous impact. This happened with the development of semiconductors for imaging techniques, like the Charge Coupled Device (CCD), and with building adaptive optics for astronomical telescopes. The opening of new spectral windows like gamma- and x-rays at short wavelengths or microwaves at long wavelengths, created whole new areas for astronomical research.

As shown, the spectropolarimetric work applied on hot stars has been quite successful. The confirmation of turbulent structures in stellar winds, equatorial density enhancements and disks, via linear polarization, and magnetic fields (dipole, or more complex, quadrupole field structures) via circular polarization are just two examples. Zeeman Doppler imaging can yield "magnetic surface maps" for different elements.

Theoretical considerations are still relatively preliminary: for instance, that multiple scattering can yield higher amounts of polarization is a very recent result.

The next step will lead in the direction of simultaneous measurements of both linear *and* circular polarized light. Combined with high signal-to-noise observations it should be possible to detect magnetic fields in other then only magnetic stars, along with the extended structures (in linear polarization) which cause them. If this will be possible a strong impact on the model of magnetically driven winds can be expected.

After spectropolarimetric "snapshots" over only a few days, long-term coverage is necessary to understand wind interactions in hot star binaries. And, finally, using the knowledge of wind stratification a better calibration of the velocity law should be attanable.

One problem still remains: the small contrast. To detect magnetic fields down to less than 100 Gauss not only in the brightest stars requires a reasonably large telescope. On the other hand, large telescopes with polarizer units do exist (e.g., ESO/CASPEC, AAT, Herschel and Keck), but generally only for linearly *or* circularly polarized light.

The development and construction of the William-Wehlau-Spectropolarimeter will give a unique opportunity to fill this gap. The weight of the polarizer unit is less than 30kg, so it is easy to transport and also small telescopes can accomodate it at the Cassegrain focus. In addition, the double-fiber can feed any standard spectrograph, which makes it usable at most observatories.

Bibliography

[1] Auer, L.H., 1987, in: W. Kalkofen (ed.), *Numerical Radiative Transfer*, Cambridge University Press, p.101

[2] Baade, D., 1984, A&A, 135, 101

[3] Barker, P.K., Landstreet, J.D., Marlborough, J.M., Thompson, I., Maza, J., 1981, ApJ, 250, 300

[4] Barker, P.K., Landstreet, J.D., Marlborough, J.M., Thompson, I., 1985, ApJ, 288, 741

[5] Behr, A, 1959, Nachr. Akad. Wissenschaften Göttingen 2, Mathem. Physik, K1, 7185

[6] Beals, C.S., 1929, MNRAS, 90, 202

[7] Bjorkman, J.E., Cassinelli, J.P., 1993, ApJ 409, 429

[8] Bjorkman, K.S., 1992, in: L. Drissen, C. Leitherer, A. Nota (eds), Nonisotropic and Variable Outflow from Stars, ASP Conference Series, Vol. 22, p. 71

[9] Brown, McLean, 1977,

[10] Cassinelli, C.P., Haisch, B.M., 1974, ApJ, 188, 101

[11] Chandrasekhar, S., 1946, ApJ, 103, 351

[12] Chandrasekhar, S., 1947, ApJ, 105, 424

[13] Chandrasekhar, S., 1950, AJ, 55, 209

[14] Chiosi, C., Meader, A., 1986, Ann. Rev. Astr. Ap., 68, 415

[15] Clarke, D., McLean, I.S., 1974, MNRAS, 167, 27P

[16] Crowther, P.A., Smith, L.J., Hillier, D.J., Schmutz, W., 1995, A&A, 293, 427

[17] Dachs, J., 1980, in: "Proc. of the 2nd Europ. IUE-Conf.", ESA-SP, 157, 139

[18] Donati, J.-F., Semel, M., Praderie, F., 1989, A&A, 225, 467

[19] Drissen, L., St.-Louis, N., Moffat, A.F.J., Bastien, P., 1987, ApJ, 322, 888

[20] Drissen, L., Robert, C., Moffat, A.F.J., 1992, ApJ, 386, 288

[21] Eversberg, T., Lépine, S., Moffat, A.F.J., 1998, ApJ, 494, 799

[22] Hall, J.S., 1949, Science, 109, 165

[23] Hanuschik, R.W., 1996, A&A, 308, 170

[24] Harries, T.J., 1995, "Spectropolarimetry as a Probe of Stellar Winds", Ph.D. thesis, University College London

[25] Harries, T.J., Howarth, I.D., 1996, A&A, 310, 553

[26] Hartwig, G., Schopper, H., 1959, Bull. Am. Phys. Soc., 4, 77

[27] Hayes, D.P., 1984, AJ, 89, 1219

[28] Hillier, D.J., 1996, A&A, 308, 521

[29] Hillier, D.J., 1996, in: S. Jeffery, U. Heber (eds.), Hudrogen Deficient Stars, Proc. 2nd Intern. Coll., in press

[30] Hiltner, W.A., 1949, Science, 109, 165

[31] Huang, S.S., 1974, ApJ, 183, 541

[32] Ignace, R., Cassinelli, J.P., Bjorkman, J.E., 1996, ApJ, 459, 671

[33] Jiang, Y.M., Walker, G.A.H., Dinshaw, N., Matthews, J.M., 1993, in: LA. Balona, H.F. Henrichs, J.M. Le Contel (eds.), Pusation, Rotation and Mass Loss in Early-Type Stars, Proc. IAU Symp. No. 163 (Dordrecht Kluwer), p.232

[34] Landstreet, J.D., 1979, AJ, 85, 611

[35] Landstreet, J.D., 1982, ApJ, 258, 639

[36] Langer, N., Hamann, W.-R., Lennon, M., Najarro, F., Pauldrach, A.W.A., Puls, J., 1994, A&A, 290, 819

[37] Lupie, O.L., Nordsieck, K.H., 1987, AJ, 92, 214

[38] Mathewson, D.S., Ford, V.I., 1970, Mem. R. Astr. Soc., 74, 139

[39] Mathys, G., Stenflo, J.O., 1986, A&A, 168, 184

[40] Mathys, G., 1991, A&AS, 89, 121

[41] Mathys, G., 1994, A&AS, 108, 547

[42] Mathys, G., 1995, A&A, 293, 733

[43] Mathys, G., 1995, A&A, 293, 746

[44] McLean, I.S., Coyne, G.V., Frecker, J.E., Serkowski, K., 1979a, ApJ, 228, 802

[45] McLean, I.S., Coyne, G.V., Frecker, J.E., Serkowski, K., 1979b, ApJ, 231, L141

[46] McLean, I.S., 1978, MNRAS, 186,

[47] Moffat, A.F.J., Piirola, V., 1993, ApJ, 413, 724

[48] Morel, T., St.-Louis, N., Marchenko, S., 1996, ApJ, submitted

[49] Motz, H., Thon, W., Whitehurst, R.N., 1953, J. Appl. Phys., 24, 826

[50] Ng, K.C., 1974, J. Chem. Phys., 61, 2680

[51] Partington, J.R., 1953, in: An advances treatise on physical chemistry, vol4, "Physico-chemical optics", Longmans, Green, New York, p. 688

[52] Nordsieck, K.H., Babler, B., Bjorkman, K.S., Meade, M.R., Schulte-Ladbeck, R.E., Taylor, M.J., 1992, in: L. Drissen, C. Leitherer, A. Nota (eds), Nonisotropic and Variable Outflow from Stars, ASP Conference Series, Vol. 22, p. 114

[53] Owocki

[54] Poeckert, R., Marlborough, J.M., 1977, ApJ, 218, 220

[55] Poeckert, R., Marlborough, J.M., 1978, ApJ, 220, 940

[56] Preston, T., 1928, "The theory of light", Macmillan, London, ed.5

[57] Robert, C., Moffat, A.F.J., 1989a, ApJ, 343, 902

[58] Robert, C., Moffat, A.F.J., Bastien,P., Drissen L., St-Louis, N., 1989b, ApJ, 347, 1034

[59] Robert, C., Moffat, A.F.J., Bastien, St-Louis, N.,P., Drissen L., 1990, ApJ, 359, 211

[60] Robert, C., Moffat, A.F.J., Drissen L., Lamontagne, R., Seggewiss, W., Niemela, V.S., Cerruti, M.A., Barrett, P., Bailey, J., Garcia, J., Tapia, S., 1992, ApJ, 397, 277

[61] Semel, M., 1989, A&A, 225, 456

[62] Semel, M., Donati, J.-F., Rees, D.E., 1993, A&A, 278, 231

[63] Schulte-Ladbeck, R.E., Nordsieck, K.H., Nook, M.A., Magalhães, A.M., Taylor, M., Bjorkman, K.S., Anderson, C.M., 1990, ApJ, 365, L19

[64] Schulte-Ladbeck, R.E., Nordsieck, K.H., Taylor, M., Nook, M.A., Bjorkman, K.S., M.A., Magalhães, A.M., Anderson, C.M., 1991, ApJ, 382, 301

[65] Schulte-Ladbeck, R.E., Nordsieck, K.H., Taylor, M., Bjorkman, K.S., M.A., Magalhães, Wolff, M.J., 1992a, ApJ, 387, 347

[66] Schulte-Ladbeck, R.E., Nordsieck, K.H., Code, A.D., Anderson, C.M., Babler, B.L., Bjorkman, K.S., Clayton, G.C., Magalhães, A.M., Meade, M.R., Shepherd, D., Taylor, M., Whitney, B.A., 1992b, ApJ, 391, L37

[67] Schulte-Ladbeck, R.E., Meade, M., Hillier, D.J., 1992, in: L. Drissen, C. Leitherer, A. Nota (eds), Nonisotropic and Variable Outflow from Stars, ASP Conference Series, Vol. 22, p. 118

[68] Schulte-Ladbeck, R.E., Eenens, P.R., Davis, K., 1995, ApJ, 454, 917

[69] Schwarzschild, M., 1950, ApJ, 112, 222

[70] Serkowski, K., 1974, in: Methods of Exp. Phys., Vol.12, Chap.8

[71] Serkowski, K., 1962, in: Advances in Astronomy and Astrophysics, 1, 247

[72] Serkowski, K., 1970, ApJ, 160, 1083

[73] Serkowski, K., Mathewson, D.S., Ford, V.L., 1975, ApJ, 196, 261

[74] Shurcliff, W, 1962, "Polarized light", Cambridge University Press

[75] Slettebak, A., 1976, in: A. Slettebak (ed.), "Be and Shell Stars", Proc. IAU Symp. No. 70 (Dordrecht Kluwer), p. 123

[76] Smith, S.J., Purcell, E.M., 1953, Phys. Rev., 92, 1069

[77] St.-Louis, N., Drissen, L., Moffat, A.F.J., Bastien, P., Tapia, S., 1987, ApJ, 322, 870

[78] St.-Louis, N., Moffat, A.F.J., Drissen, L., Bastien, P., Robert, C., 1988, ApJ, 330, 286

[79] St.-Louis, N., Moffat, A.F.J., Lapointe, L., Efimov, Yu.S., Shakhovskoy, N.M., Fox, G.K., Piirola, V., 1993, ApJ, 410, 342

[80] St.-Louis, N., Dalton, M.J., Marchenko, S.V., Moffat, A.F.J., Willis, A.J., 1995, ApJ, 452, 57

[81] Struve, O., 1931, ApJ, 73, 94

[82] Taylor, M., 1992, in: L. Drissen, C. Leitherer, A. Nota (eds), Nonisotropic and Variable Outflow from Stars, ASP Conference Series, Vol. 22, p. 57

[83] van der Hucht, K.A., 1994, in: K.A. van der Hucht & P.M. Williams (eds.), Wolf-Rayet Stars: Binaries, Colliding Winds, Evolution, Proc. IAU Symp. No. 163 (Dordrecht: Kluwer), p.7

[84] Willis, A.J., 1991, in: K.A. van der Hucht & B. Hidayat (eds.), Wolf-Rayet Stars and Interrelations with Other Massive Stars in Galaxies, Proc. IAU Symp. No. 143 (Dordrecht: Kluwer), p.265

[85] Wood, K., Brown, J.C., Fox, G.K., 1993, A&A, 271, 492

[86] Wood, K., Bjorkman, J.E., Whitney, A., Code, A.D., 1996, ApJ, 461, 828

Postscriptum

During the annual Hot Star Meeting of the Universities of Newark/Delaware and Montreal/Quebec in June 1996, Owocki (1996, in preparation) presented new results of numerical calculations for fast rotating oblate Be stars. In these calculations non-radial line-forces are also considered.

In disagreement with the Wind Compressed Disk Model of Bjorkman & Cassinelli, who assumed a radial-symmetric line-force, Owocki's calculations *can not create an equatorial disk*!

That means, the observed disk is still *not well explained* and magnetic fields, possibly measureable with spectropolarimetric tools, could be the key for understanding Be stars.